hexagon:2611.00410v1

VERIFICATION OF THE MARKOV UNIQUENESS CONJECTURE FOR THE FIRST ONE TRILLION MARKOV VALUES: MERIDIANS ON THE MARKOV SURFACE AND FAREY ADDRESSES

ELLEARD FELIX WEBSTER HEFFERN

Abstract. The Markov unicity problem asks whether the largest entry of a positive integer solution determines the other two. We organize the triples into families called Meridians, with compact addresses and explicit evaluation rules. The construction starts with catenary profiles: a fixed host sets the curve, and two heights one unit apart solve the Markov equation with that host. Selected positions give integer triples. Reversing geometric descent gives an exact indexing of these triples. Remainder patterns, growth bounds, corridor paths, and Fibonacci-matrix and snake-graph arguments then restrict possible collisions.

The Meridian description of starting scales and logarithmic spacing guided the organization of a large verification into magnitude bands. The implementation uses Farey addresses and certified matrix bounds to select each band; its correctness does not require the Meridian collision theorems. Production finished on 10 November 2026 at 03:54:13 UTC (9 November, 21:54:13 CST). The combined computation compared 1,101,388,071,945 configurations and certified uniqueness of the first one trillion Markov values in numerical order. The trillionth value has 1,021,609 decimal digits. All 12 repeated 64-bit residue groups were resolved by exact arithmetic, with no equal maxima. On eight workers, retained active band processing took 23 h 57 min 23.146 s, including the inherited 500-billion certificate; the maximum recorded temporary key-file footprint was 1,065,664,392 bytes (0.992 GiB). This elapsed processing time is distinct from summed CPU time and the calendar span. Both final replays passed. A separate computer-checked certificate covers all 5,067,077 Meridians of degree at most 10,000, at every integer phase. The general unicity problem remains open.

1. Introduction

A Markov triple consists of three positive integers satisfying

$$a^2 + b^2 + M^2 = 3abM, \qquad 1 \le a \le b \le M. \tag{1}$$

For example, $(1, 2, 5)$ and $(1, 5, 13)$ are Markov triples. The largest entry of such a triple is a Markov number. The *unicity problem* asks a simple question: does that largest entry determine the other two? A counterexample would consist of two different ordered triples with the same largest entry. We call such an equality a *collision*. For the history and wider setting of the problem, see Aigner [9]. An early computational benchmark is due to Baragar [8, Section 4, p. 9], who reported 18,906 Markoff numbers below 10^{140} and no counterexample to unicity among all triples with maximal element less than 10^{140}.

Our starting point is to let the entries vary continuously. We build a curve on which the Markov equation holds automatically, then ask which positions give integer entries. This separates the equation itself from the requirement that its solutions be integers. It also gives a picture of what a collision would have to look like.

A second aim is practical: understand where a family of triples begins and how its values grow. The Meridian viewpoint guided our choice to compare candidates in limited size ranges, so that completed batches could be cleared from working storage. The resulting verifier uses Farey addresses

Date: Version 22 — 12 November 2026.

2020 *Mathematics Subject Classification.* Primary 11D25; Secondary 11B39, 05C70, 11Y50.

Key words and phrases. Markov numbers, unicity, geometric descent, Meridians, corridors, snake graphs.

and certified matrix bounds to select those batches. It compares more than 1.1 trillion configurations and certifies the first one trillion values in numerical order.

1.1. **The host and its catenary profile.** The *host* h is the fixed third entry around which we build the curve. It determines a profile f_h: two heights on this profile, taken one horizontal unit apart, will satisfy the Markov equation together with h. We first allow positive real entries and call any such solution a *real Markov state*. The host need not yet be an integer or the largest entry; those requirements will be imposed when we return to the unicity question.

For $h > 2/3$, define

$$q_h = \frac{3h}{2}, \qquad R_h = \sqrt{q_h^2 - 1}, \qquad Q_h = q_h + R_h, \tag{2}$$
$$f_h(x) = \frac{h}{2R_h}(Q_h^x + Q_h^{-x}).$$

The restriction $h > 2/3$ makes R_h positive and $Q_h > 1$; it includes every positive integer host. The graph of f_h is a rescaled catenary: a smooth, symmetric U-shaped curve, with its minimum at $x = 0$. In particular, $f_h(-x) = f_h(x)$. In (2), x is a free position on this profile. We use c below for a particular selected position.

The constants in (2) set the spacing and height scale so that one horizontal unit has the required arithmetic meaning. The calculation is short. First,

$$(q_h + R_h)(q_h - R_h) = q_h^2 - R_h^2 = 1,$$

so

$$Q_h^{-1} = q_h - R_h, \qquad Q_h + Q_h^{-1} = 3h, \qquad Q_h - Q_h^{-1} = 2R_h.$$

These three identities follow directly from the definitions.

1.2. **Why two heights one unit apart satisfy the equation.** Compare $f_h(x+1)$ with $Q_h f_h(x)$. The terms containing Q_h^{x+1} cancel, leaving

$$\begin{aligned} f_h(x+1) - Q_h f_h(x) &= \frac{h}{2R_h}(Q_h^{-x-1} - Q_h^{1-x}) \\ &= \frac{h}{2R_h} Q_h^{-x}(Q_h^{-1} - Q_h) = -hQ_h^{-x}. \end{aligned}$$

Multiplying $f_h(x)$ by Q_h^{-1} instead cancels the terms containing Q_h^{-x-1}:

$$\begin{aligned} f_h(x+1) - Q_h^{-1} f_h(x) &= \frac{h}{2R_h}(Q_h^{x+1} - Q_h^{x-1}) \\ &= \frac{h}{2R_h} Q_h^{x}(Q_h - Q_h^{-1}) = hQ_h^{x}. \end{aligned}$$

Now multiply these two equalities. The powers on the right cancel:

$$\big(f_h(x+1) - Q_h f_h(x)\big)\big(f_h(x+1) - Q_h^{-1} f_h(x)\big) = -h^2.$$

Expanding the left side gives

$$f_h(x+1)^2 - (Q_h + Q_h^{-1}) f_h(x) f_h(x+1) + f_h(x)^2 = -h^2.$$

Finally, use $Q_h + Q_h^{-1} = 3h$ and move h^2 to the left:

$$\boxed{f_h(x)^2 + f_h(x+1)^2 + h^2 = 3f_h(x)f_h(x+1)h.} \tag{3}$$

Thus *every* real position x gives a real Markov state. No choice of an integer value or a special position was used in this calculation.

1.3. **Choosing an integral state: the role of c.** To look for an ordered triple with largest entry h, select $0 < c \le 1/2$ and take the unit interval $[c-1, c]$ across the bottom of the curve. Its two heights are $f_h(c-1)$ and $f_h(c)$. By symmetry, $f_h(c-1) = f_h(1-c)$, so the state, with its companions in increasing order, is

$$(f_h(c),\ f_h(1-c),\ h).$$

It solves the equation by (3), with $x = c - 1$. For it to be a normalized Markov triple, h and both heights must be positive integers, and $f_h(1-c) \le h$ must hold. The latter condition keeps the chosen host as the largest entry. Restricting c to this half of the unit interval avoids counting the reflected pair twice.

Figure 1 shows the distinction for $h = 5$. One choice, $c \approx 0.351515$, gives the heights 1 and 2, hence the integer triple $(1, 2, 5)$. A different choice, $d = 0.44$, gives heights approximately 1.207458 and 1.602614. It still solves the same equation with host 5, but its companion heights are not integers.

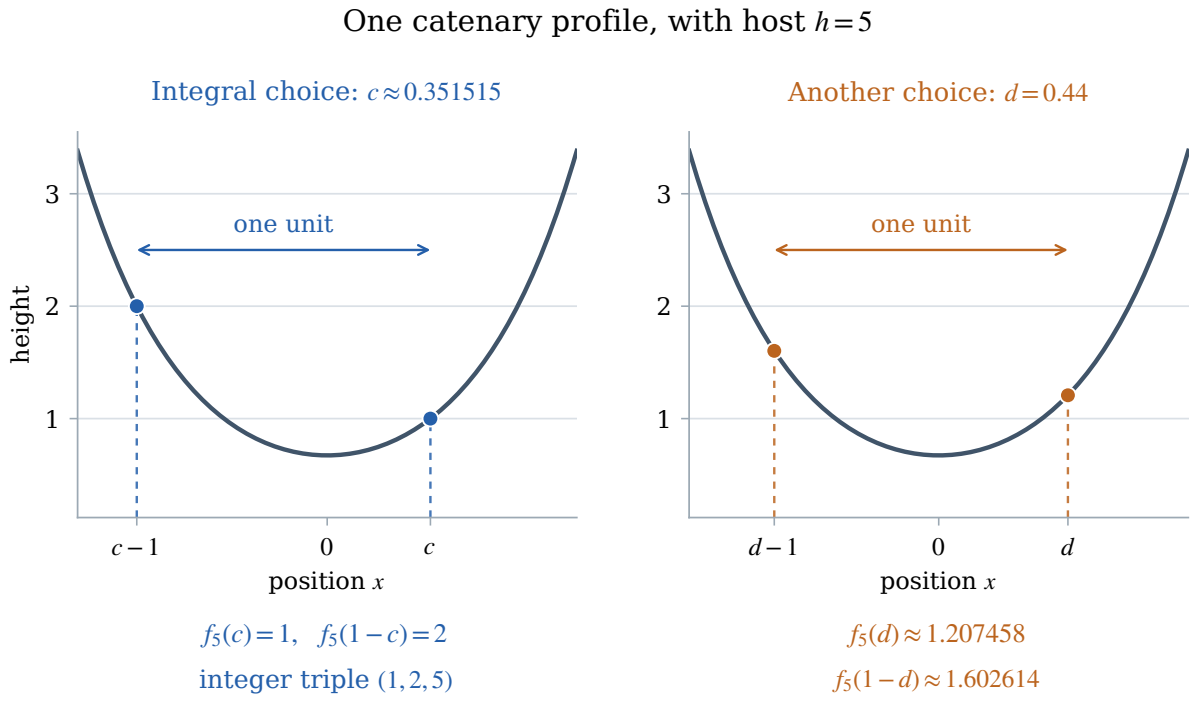


Figure 1. Two choices on the same catenary profile, with host $h = 5$. In each panel the marked contacts are exactly one horizontal unit apart. The left contact has height $f_5(1-c)$ or $f_5(1-d)$ by symmetry. The choice c gives an integer triple; the displayed choice d gives only a real state. A collision would require two distinct choices with both pairs of heights integral and with the same host as their largest entry. No collision is shown here.

This is the geometric form of the unicity question. For a fixed integer host h, could two distinct choices c and d in $(0, 1/2]$ both give integer companion heights no larger than h? If so, they would give different ordered triples with the same maximum. The curve makes these possible comparisons visible. To exclude them requires information about the integer values on the curve.

1.4. **How the paper organizes those comparisons.** The next step is *descent*. Starting from two contact heights, we look for a smaller host whose profile passes through the same heights one unit

apart. We then move inward along that profile. Repeating these operations reduces a normalized integer Markov triple to $(1, 1, 1)$. Section 2 makes the procedure precise and explains how its final host and final position recognize the integer starting states.

Reversing the steps organizes the triples into families called *Meridians*. Each family has an address recording the steps used to construct it, and a phase specifying a position along it. This Meridian phase is a separate coordinate from the selected c on a fixed catenary. Integer Meridian phases pick out integer triples; the corresponding c need not be an integer, as Figure 1 shows. Section 3 proves that these addresses and integer phases recover every normalized triple exactly once. This is a statement about triples: whether two of them have the same largest entry remains the question to be answered. The same section introduces the alternative tree and the *phasors* that connect its Meridians.

The remainders of the Markov values follow exact periodic patterns (Section 4). Section 5 then develops the ordering tools used in the collision arguments. It represents Markov numbers by counts of perfect matchings on chains of square tiles, called snake graphs; a perfect matching pairs all the vertices using edges of the graph. The author's Fibonacci matrices and six-piece decomposition provide concrete ways to compare these counts.

The following two sections use those constructions to control growth. A Meridian's *degree* measures the largest exponent in its formula. We prove that distinct integer marks of the same degree cannot collide. For different degrees, a positive expansion of the Fibonacci blocks gives a finite range of phases that needs comparison (Section 6). *Corridor walls* follow other paths through the same tree, using both Meridian and phasor steps. Adding one to each Fibonacci run index gives their recurrence and a second bound on possible collisions (Section 7).

The resulting computer-checked certificate covers all 5,067,077 Meridians of degree at most 10,000, at every integer phase (Theorem 8.1). Distinct triples within that family have different maxima. This bounds the complexity of the families, while allowing their values to grow without limit; comparisons with higher-degree Meridians remain outside this certificate. Section 9 records the separate numerical-order verification. Meridian helms and degree-dependent logarithmic spacing motivated its organization by scale. The production code implements that organization through groups of Farey addresses with shared, certified size bounds; it does not schedule one Meridian at a time. The same band algorithm can be formulated entirely in Farey and matrix terms. Its finite-prefix conclusion does not use the Meridian collision exclusions, and the timings do not isolate a speedup due to the change of coordinates alone. It compared 1,101,388,071,945 configurations and certified uniqueness of the first one trillion values, including every possible competitor at those values. Production finished on 10 November 2026 at 03:54:13 UTC (9 November, 21:54:13 CST), using 23.956 hours of retained active band processing, including the inherited work, and at most 0.992 GiB of recorded temporary key files. Both final replays passed. The section gives the exact timing and storage scopes, together with the earlier fifty-billion result. The general unicity problem remains open within this framework.

As the later sections introduce their coordinates, $M_\alpha(x)$ will denote the value at Meridian address α and phase x, and $m_{p/q}$ the value of the triple indexed by the reduced fraction p/q. Both label triples before any assertion that their maxima are distinct. Analytical logarithms are natural; plotted horizontal axes use $\log_{10} M$.

2. Geometric descent and arithmetic closure

2.1. **Moving along a profile and changing its host.** The catenary profile (2) turns two elementary operations on Markov states into movements of the contacts. The first operation is a

unit step along a fixed profile. Directly from its powers,

$$f_h(x+1)+f_h(x-1)=\frac{h}{2R_h}(Q_h+Q_h^{-1})(Q_h^x+Q_h^{-x}) \\ =3hf_h(x). \tag{4}$$

Thus the height beyond a pair is obtained by multiplying the nearer height by $3h$ and subtracting the farther height. This is the usual Vieta replacement of a companion entry, expressed on the curve.

The second operation keeps the contact heights fixed and changes the host. For any real x, put $A=f_h(x)$ and $B=f_h(x+1)$. Their possible hosts are the roots of $X^2-3ABX+A^2+B^2=0$. One root is h, so the other is

$$h, \qquad K=3AB-h=\frac{A^2+B^2}{h}. \tag{5}$$

For descent, select an edge straddling the minimum of the profile. We record its right endpoint as c, with $0\le c<1$, and its ordered contact heights as $A=f_h(c)$ and $B=f_h(c-1)$. This is the same pair used in the introduction, since $f_h(c-1)=f_h(1-c)$. We retain the full interval of c here to keep track of orientation. Seek a wider profile through these same two heights, still one unit apart, allowing a horizontal translation. Smaller h gives a wider profile. If the other host satisfies $K<h$, fit that profile and walk the unit lattice inward until the selected edge again straddles its vertex. Otherwise stop. Figure 2 shows one complete step. The fit is explicitly

$$v=\frac{\log((Q_KA-B)/K)}{\log Q_K}, \qquad f_K(v)=A, \quad f_K(v-1)=B. \tag{6}$$

Indeed, $Q_Kf_K(v)-f_K(v-1)=KQ_K^v$, so taking logarithms recovers v directly. The Markov relation gives

$$(Q_KA-B)(B-Q_K^{-1}A)=K^2.$$

Both factors are positive: they have the same sign, and their sum is $2R_KA>0$. This also fixes the real branch of the logarithm and verifies the fitted contact heights by direct substitution. The walk replaces v by $v-\lfloor v\rfloor$. Its orientation is retained: reflection exchanges the contacts and sends phase to its negative modulo one.

Proposition 2.1 (Uniqueness of the fit)**.** *A marked edge has at most one distinct compatible profile, hence at most one wider fit. For fixed $0<a<b$, a same-arm fit $f_h(u-1)=a$, $f_h(u)=b$ with $u>1$ is unique if it exists.*

Proof. The hosts are the two roots of $X^2-3ABX+A^2+B^2$. The other root belongs to the geometric domain because $(3K-2)AB=K^2+(A-B)^2>0$. For a same-arm fit the horizontal distance between heights a,b is

$$\frac{1}{\log Q_h}\int_a^b\frac{dy}{\sqrt{y^2-h^2/R_h^2}}.$$

When $a>2/3$ and the lower height is in range, Q_h strictly increases and $h/R_h=2h/\sqrt{9h^2-4}$ strictly decreases with h. Thus the prefactor and the integrand strictly decrease with h. The distance can therefore equal one at most once. The profile is strictly increasing on that arm, which also determines u. If $a\le 2/3$ there is no fit. □

2.2. **Termination.** Write $\mathcal{D}(M,c)=(H,\phi)$ for the terminal host and oriented phase.

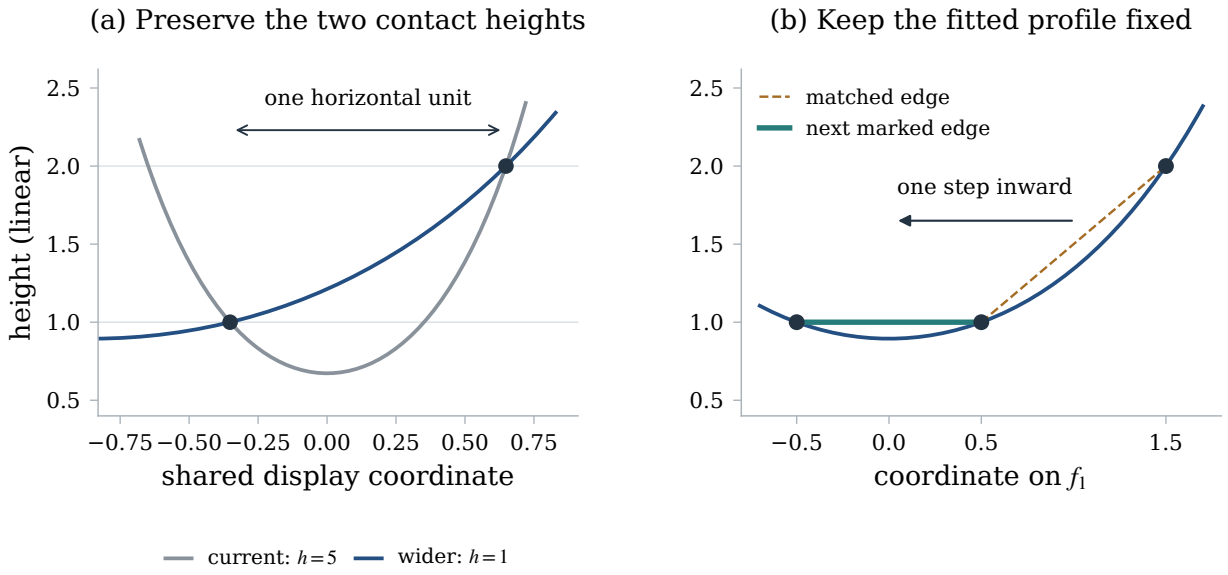


Figure 2. Geometric descent from $(1, 2, 5)$. The wider profile passes through the same unit-spaced contacts. On f_1 their coordinates are $1/2, 3/2$; one inward step selects $-1/2, 1/2$, with heights $1, 1$. The curve is fixed during the walk.

Theorem 2.2 (Finite descent)**.** *Every straddling input with $M \geq 1$ terminates. On $1 \leq M \leq R$ the number of host changes is uniformly bounded. The terminal map is continuous into $(2/3, \infty) \times \mathbb{R}/\mathbb{Z}$ and analytic on cells with a fixed strict itinerary.*

Proof. Temporarily sort the endpoints as $a \leq b$. Inward walking does not increase either endpoint. Every current host is at most R, and the discriminant in (3) gives

$$(9h^2 - 4)a^2 - 4h^2 = (2b - 3ha)^2 \geq 0.$$

Consequently the endpoints are at least $a_R = 2R/\sqrt{9R^2 - 4} > 2/3$. At an accepted change, $a^2 + b^2 < h^2$, so the endpoints are also below $h \leq R$. Using either endpoint as the host in the same discriminant identity bounds the new host below by a_R. The initial host is at least $1 > a_R$.

If the new host K is at least b, its edge already straddles the vertex, because both endpoints are below $f_K(1)$; the next candidate is the old, larger host, so descent stops. Otherwise

$$\frac{h}{K} > \frac{h}{b} = 3a - \frac{K}{b} > 3a - 1 \geq 3a_R - 1 > 1.$$

All changes except possibly the last therefore contract the host by a fixed factor. An upper bound is $1 + \lceil \log(R/a_R)/\log(3a_R - 1) \rceil$.

At a boundary $K = h$, the fitted coordinate in (6) is the original c, so the accepted and stopped maps agree. At a phase cut, $K(h, 0) = h(9h^2 + 4)/(9h^2 - 4) > h$, and a neighborhood is stopped. The uniform bound on compositions then gives continuity, with phase taken modulo one. The strict formulas are analytic. □

2.3. **Which inputs close arithmetically?** The two reversible state operations are

$$T(a, b, h) = (3ha - b, a, h), \qquad J(a, b, h) = (a, b, 3ab - h). \tag{7}$$

They and their inverses are integer polynomial maps. A terminal state has the nonnegative defect

$$H f_H(\phi) f_H(\phi-1) - 1 = \frac{(H-1)^2(H+2)}{3H-2} + \frac{H^3}{4R_H^2}\left(Q_H^{\phi-1/2} - Q_H^{1/2-\phi}\right)^2. \tag{8}$$

For $0 \le \phi < 1$ it vanishes exactly at $(H, \phi) = (1, 1/2)$.

Proposition 2.3 (Arithmetic closure)**.** *A straddling input with $M \ge 1$ reaches $(1, 1/2)$ if and only if its three entries are positive integers. Modulo companion exchange, these inputs are exactly the normalized configurations* (1)*.*

Proof. Expanding the two profiles gives

$$H f_H(\phi) f_H(\phi-1) - 1 = \frac{H^3}{4R_H^2}\left(Q_H^{2\phi-1} + Q_H^{1-2\phi} + 3H\right) - 1.$$

Replace the first two powers by $\left(Q_H^{\phi-1/2} - Q_H^{1/2-\phi}\right)^2 + 2$. The constant term is $H^3/(3H-2) - 1 = (H-1)^2(H+2)/(3H-2)$, which proves (8). Reversing a finite closure itinerary from $(1,1,1)$ by (7) preserves integrality. Conversely, integral descent stays integral. At an integral terminal state order the entries as $u \le v \le w$. There is no coordinate-decreasing mutation. But for $Q(X) = X^2 - 3uvX + u^2 + v^2$,

$$Q(v) = u^2 + (2-3u)v^2 \le 3u^2(1-u) \le 0.$$

If neither root is below $w \ge v$, equality is forced, giving $u = v = 1$; terminality then gives $w = 1$. Finally, a straddling edge has no decreasing endpoint mutation, so its host is a largest entry. Its ordered split is uniquely recovered by (6). □

Both terminal coordinates matter. Figure 3 shows inputs with terminal host one but different terminal phases. A crossing of the height level $H = 1$ alone does not certify integrality. The marked configurations follow the host itineraries $37666 \to 5 \to 1$, $7561 \to 5 \to 1$, and $14701 \to 2 \to 1$, all ending at phase $1/2$.

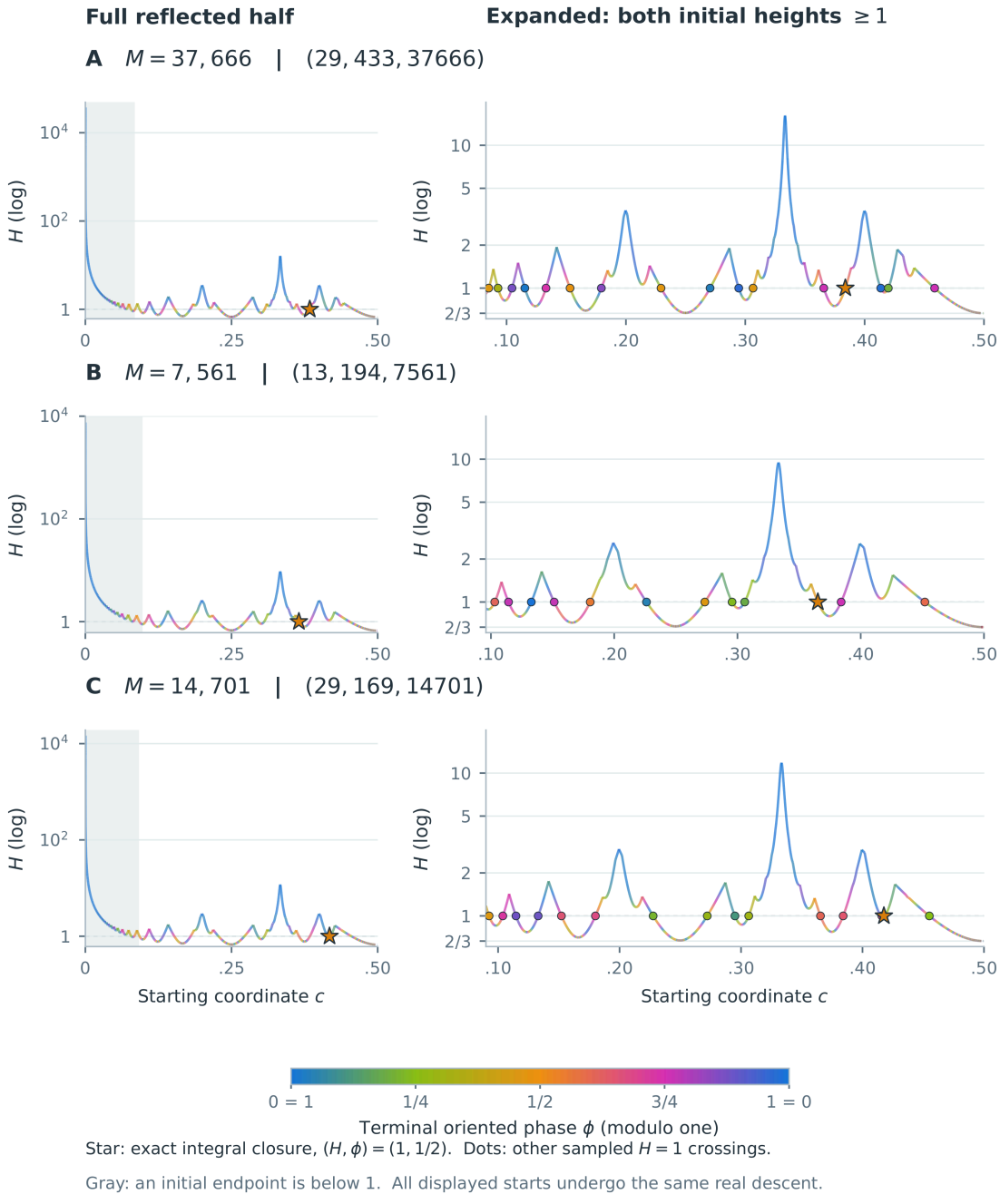


Figure 3. Terminal host and phase for $M = 37666, 7561, 14701$. Height is H on a logarithmic scale and hue is oriented phase. Left: $0 \le c \le 1/2$, with gray where an initial endpoint is below one. Right: the admissible portion enlarged. Stars mark the exact integral starts; dots are other numerically located $H = 1$ crossings. These numerical plots illustrate the closure criterion.

3. Meridians, addresses, and the alternative tree

3.1. **The landscape and its two coordinates.** On the landscape $(\log_{10} M, c)$, the point (M, c) represents the contacts $f_M(c), f_M(c-1)$. We draw the reflected half $0 < c \le 1/2$; exchanging the contacts sends c to $1-c$. A *Vieta arc* keeps one initial contact height fixed. For example, the branch with height a has

$$c = \frac{\log\Big((R_M a + \sqrt{R_M^2 a^2 - M^2})/M\Big)}{\log Q_M}.$$

This follows by solving $Q_M^c + Q_M^{-c} = 2R_M a/M$ for $Q_M^c \ge 1$ and taking logarithms. The square root is real exactly when $a \ge M/R_M$, the minimum height of the profile; reflection supplies the other arm. A *Vieta trek* follows such arcs, changing the retained contact when necessary. A *Meridian* is a connected component of terminal host $H(M, c) = 1$. A *phasor* holds the terminal phase ϕ fixed. The alternative tree uses phasors at $\phi = 1/2$ to join successive Meridians.

The address phase x on a Meridian is real and unrolled. Its terminal circle phase is $\phi \equiv x + 1/2 \pmod 1$. Every integer mark therefore closes arithmetically; the distinguished arrival mark $x = 0$ is called the *helm*. It need not be the minimum of the real profile.

Figure 4 keeps the same configurations in three views. The alternative tree is in the middle panel. The bottom panel uses smooth schematic connectors for the Vieta parent relation: node coordinates and adjacency are exact, but those connectors are not literal level curves. The two trees each have 55 edges. An unmarked crossing is not a vertex.

For reproducibility, the field in panel (a) uses the fixed cyclic phase palette with HSL saturation and lightness

$$w(H) = \frac{1}{1 + (\ln H/\ln 1.05)^2}, \qquad S = w(H), \qquad L = 1 - 23w(H)/40.$$

The background is a numerical illustration, independent of all exact enumerations and exclusions below.

3.2. **Evaluating an address.** The seed Meridian is

$$\begin{aligned} a_1(x) = f_1(x + \tfrac{1}{2}), \qquad b_1(x) = f_1(x - \tfrac{1}{2}), \\ M_1(x) = 3a_1(x)b_1(x) - 1. \end{aligned} \tag{9}$$

For integer x, its companions are F_{2x+1}, F_{2x-1}, where $F_{-j} = (-1)^{j+1}F_j$. Hence

$$M_1(x) = 2 + 3F_{2x}^2, \qquad M_1(0), M_1(1), M_1(2), \ldots = 2, 5, 29, 194, \ldots. \tag{10}$$

From any ordered state (a, b, H) form the two-sided orbit

$$u_0 = a, \quad u_1 = b, \qquad u_{j+1} = 3Hu_j - u_{j-1}.$$

A nonzero index k replaces the state by

$$(u_k, u_{k+1}, 3u_k u_{k+1} - H). \tag{11}$$

The address is written

$$\alpha = (1, k_m, \ldots, k_1): \quad k_1 \text{ is applied first and written at the right.}$$

This is the reversed indexing convention: the former $M_{1,a,b,c}(x)$ is now $M_{1,c,b,a}(x)$. Neither the signs nor x are reversed. In terms of (7), with $S = T^{-1}$ and $\mathcal{W}_k = JS^k$,

$$(a_\alpha(x), b_\alpha(x), M_\alpha(x)) = \mathcal{W}_{k_m} \cdots \mathcal{W}_{k_1} JT^x(1, 1, 1). \tag{12}$$

Composition acts from right to left. A recursive extension inserts its index immediately after the leading 1. For example, $M_{1,1}(0) = 13$. Index zero is forbidden because (11) would return the preceding pole $3ab - H$, rather than create a new component.

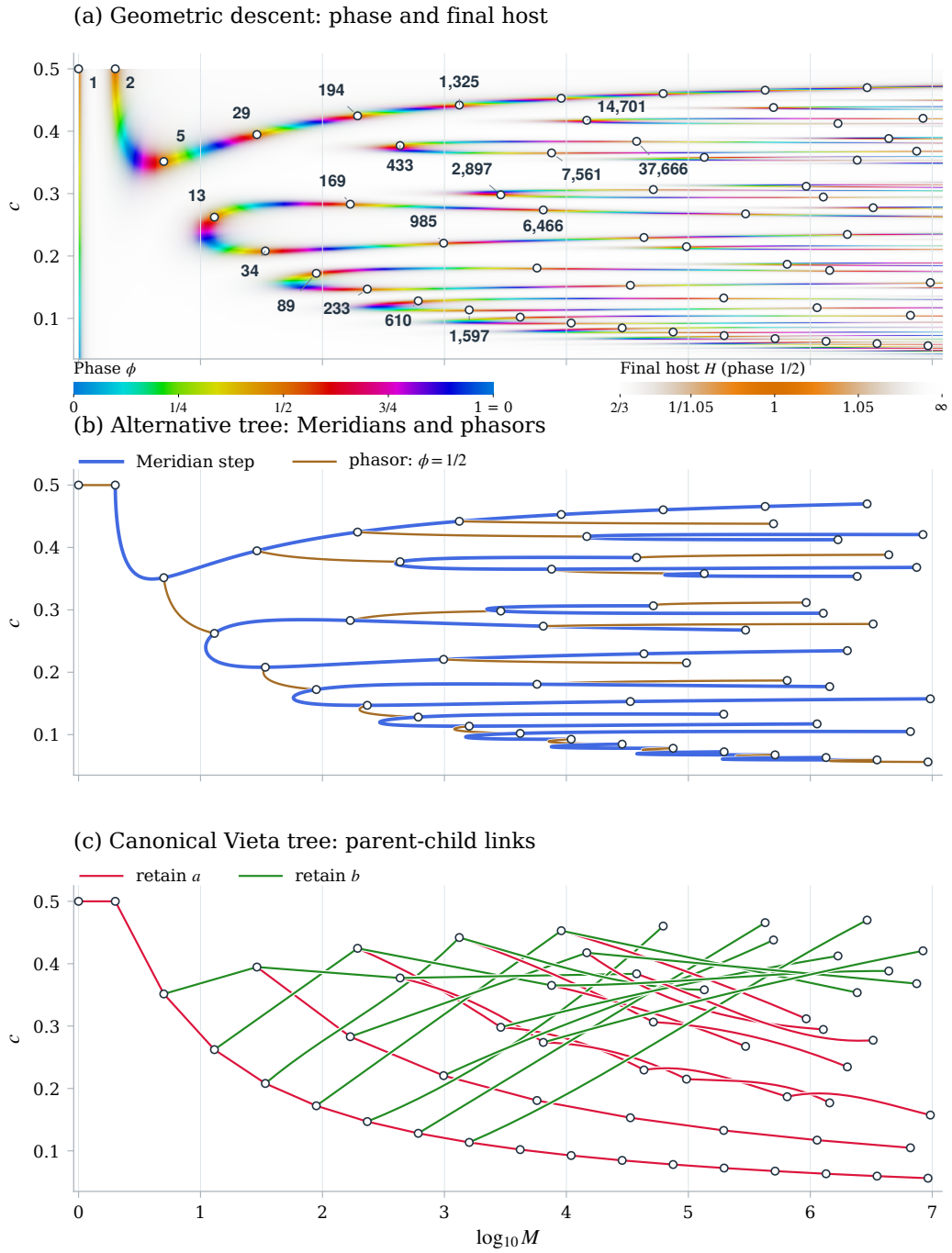


Figure 4. The same 56 configurations with $M \leq 10^7$. (a) Numerical geometric descent, with phase encoded by hue and host by color intensity. The number labels identify the same 20 Markov numbers shown in Figure 5. (b) The alternative tree, with Meridian and phasor edges. (c) The canonical Vieta tree, with simplified connectors retaining exact endpoints. Red retains the smaller companion, green the larger. Every edge runs toward larger M. Crossings without a node mark are not vertices.

Definition 3.1 (Canonical marks)**.** The root $(1,1,1)$ is separate. For the seed (1) use integer phases $x \geq 0$. For every other address require $k_1 > 0$, $k_i \neq 0$ for $i > 1$, and $x \in \mathbb{Z}$. Evaluation is followed by sorting the two companions.

Theorem 3.2 (Configuration bijection)**.** *Canonical marks are in bijection with all normalized positive Markov triples except the root. The displayed value $M_\alpha(x)$ is the largest entry.*

Proof. The quadratic argument in Proposition 2.3 shows that replacing the largest coordinate by its other pole gives a smaller maximum, apart from the initial repeated entries. This is the forced Vieta reduction of a configuration and does not assume scalar unicity.

To recover a word, reflect the current maximum H to $P = 3ab - H$. When $P \geq 2$, walk its oriented endpoint orbit inward until both endpoints are below P. This edge is unique. Indeed $u_{j+1} - 2u_j + u_{j-1} = (3P-2)u_j > 0$, so the entries below P form an interval; three consecutive entries below P would contradict $u_{j-1} + u_{j+1} = 3Pu_j \geq 3P$. Endpoint descent supplies the edge, and its nonzero signed displacement recovers the last-applied, leftmost index. Repeat at the smaller pole. At pole one, the orbit reaches $(1,1)$ and fixes the seed phase.

Conversely, all outward blocks are positive and reduced. If the preceding pole is $P < H$, the first reflected poles on the two sides are $(9b^2-2)H - P > 6H$ and $(9a^2-2)H - P > 6H$. Their farther endpoints exceed $2H$, and the recurrence makes subsequent outward entries increase. The reduction therefore undoes every prescribed block. Finally, companion exchange negates all indices and x simultaneously. The canonical conditions select one of the two orientations; only $(1,1,2)$ is fixed. □

This bijection is useful computationally as well as geometrically. A configuration can be retained by its address and reconstructed when a comparison needs its full integer entries. Section 9 uses the equivalent reduced-fraction labels as compact identities, with compressed Vieta evaluation. Its coverage therefore counts triples before testing whether their maxima are distinct.

3.3. **The two parent rules.** At a nonzero phase the alternative parent is the adjacent inward mark, $(\alpha; x) \mapsto (\alpha; x - \operatorname{sgn} x)$. At a nonseed helm it is

$$(1, k_m, \ldots, k_2, k_1; 0) \longmapsto (1, k_m, \ldots, k_2; -k_1), \tag{13}$$

followed by simultaneous sign reflection if the remaining rightmost index is negative. An empty tail uses the seed's nonnegative phase. The seed helm with maximum two has parent $(1,1,1)$.

The alternative parent deletes the *rightmost* index at a helm. Recursive evaluation removes the *leftmost* index after 1. These operations serve different purposes. The depth

$$d(\alpha; x) = 1 + \sum_{i=1}^{m} (|k_i| + 1) + |x| \tag{14}$$

decreases by one under either parent edge, with root depth zero. Thus the parent rule defines a rooted tree on the same configurations. The ordinary outward Vieta moves instead are

$$(a, b, M) \longmapsto (a, M, 3aM - b), \qquad (a, b, M) \longmapsto (b, M, 3bM - a). \tag{15}$$

For example, $29 \to 194$ is a Meridian edge, whereas $29 \to 169$ is a Vieta edge. Figure 5 compares the two sets of links.

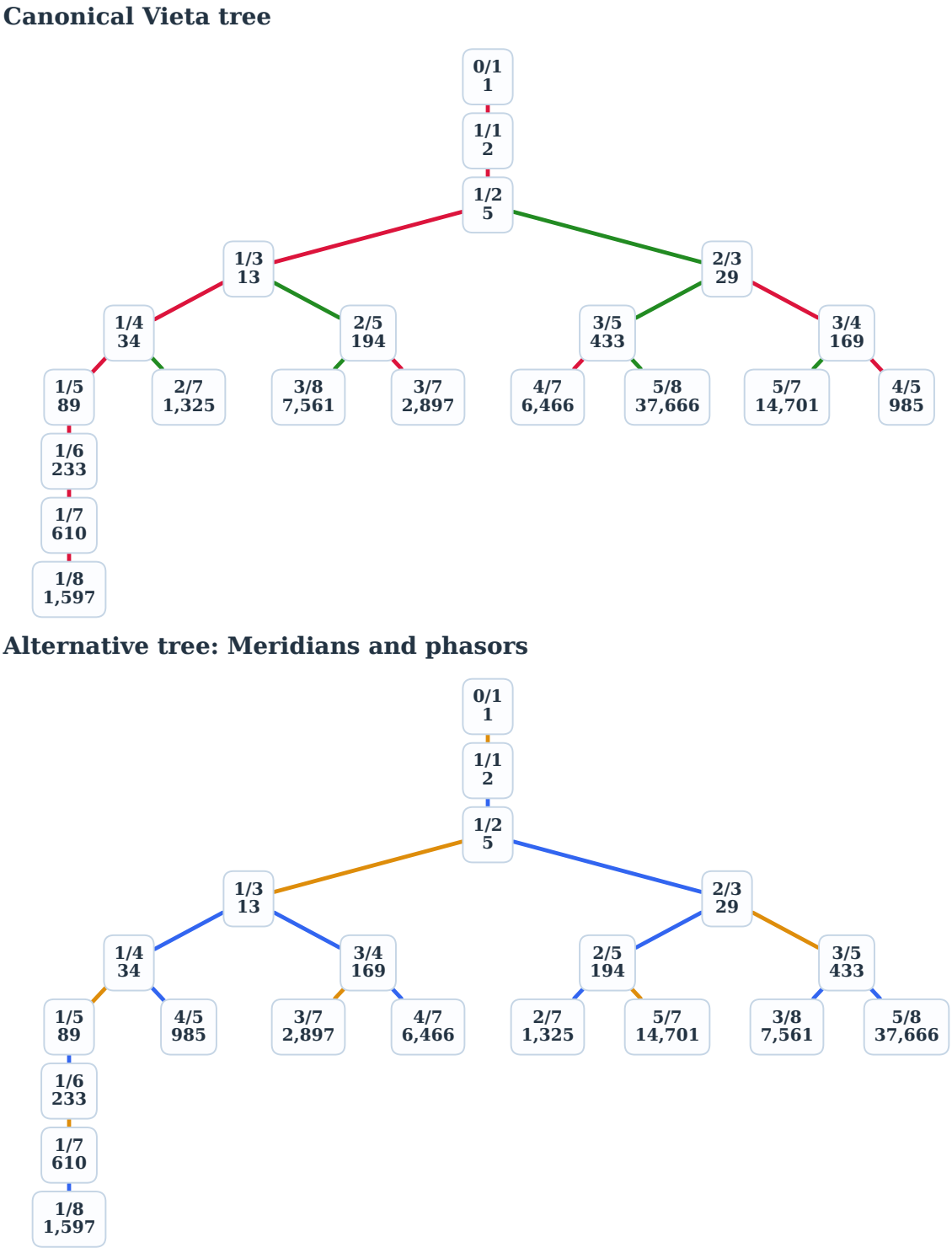


Figure 5. Two trees on the same 20 configurations: the 16 with $M \leq 3000$ and the four additional values $6466, 7561, 14701, 37666$. Each node displays its reduced standard Farey label and maximum. Red and green denote the Vieta moves; blue and gold denote Meridian and phasor steps.

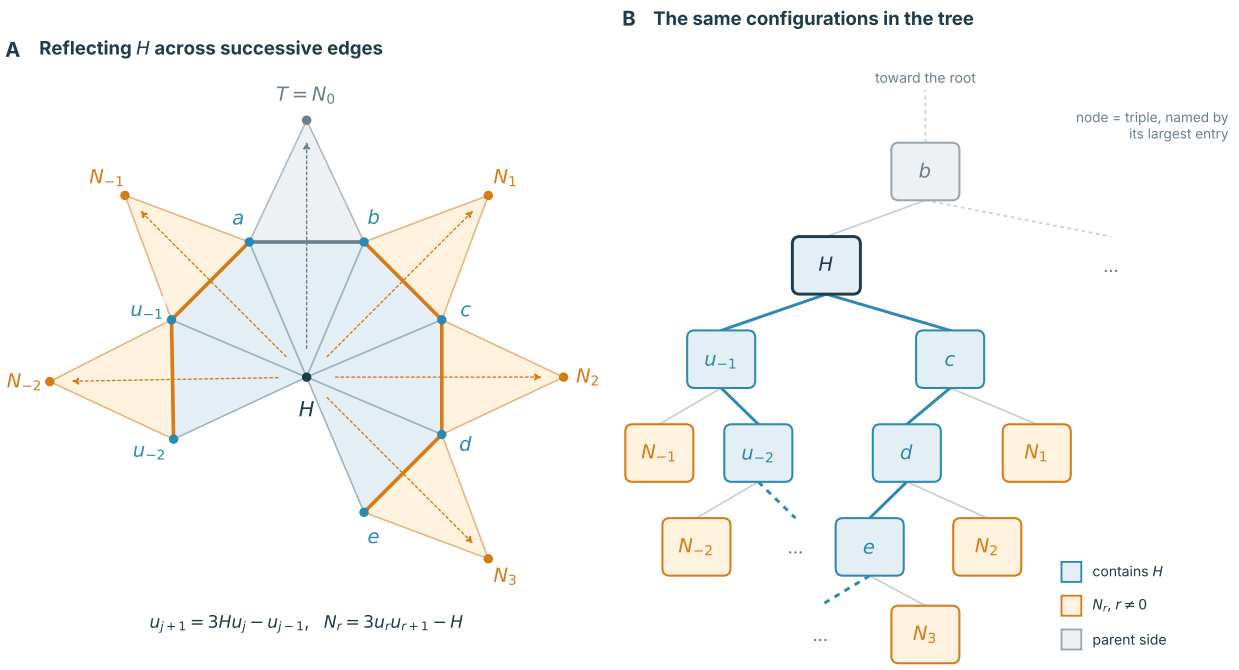


Figure 6. The orbit underlying one recursive extension. Reflecting H across (u_j, u_{j+1}) gives $N_j = 3u_ju_{j+1} - H$; N_0 is the preceding pole. For source $(a, b, H) = (1, 5, 13)$ at $M_{1,1}(0)$, the preceding pole is two, $(u_{-2}, u_{-1}, u_2, u_3, u_4) = (1325, 34, 194, 7561, 294685)$, and $(N_{-2}, N_{-1}, N_1, N_2, N_3) = (135137, 89, 2897, 4400489, 6684339842)$. The right panel locates these reflections in the Vieta tree.

3.4. **Real components and phasor edges.**

Proposition 3.3. *The canonical real families in* (12)*, modulo companion reflection, are the nonterminal connected components of* $H(M, c) = 1$*. Their terminal phase is* $x + 1/2$ *modulo one. The separate terminal component is* $M = 1$*.*

Proof. The seed companions are at least $2/\sqrt{5}$, and $M_1 \geq 2$ is strictly larger than either. More generally, let $h \geq 1$ and $2/\sqrt{5} \leq a, b \leq h$. The first outward endpoint satisfies $3hb - a \geq (6/\sqrt{5} - 1)h > h$; its reflected pole is larger still. The reversed orbit gives the same conclusion on the other side. Every outward block thus has a strict inverse descent to its source and preserves the terminal phase.

Conversely, reverse any descent ending at host one. Its last host change produces the seed with $x = v - 1/2$, and every preceding walk is nonzero: a zero walk would simply have stopped at the smaller host. These strict blocks uniquely recover a locally constant word. The unrolled x joins the final phase charts continuously. The seed is injective as an ordered curve, as its endpoint difference is strictly monotone; each block is invertible. The positive Laurent expansion proved in Proposition 6.2 makes every family proper. The inverse charts are relatively open in the level set, and properness makes the families closed. Each connected family therefore fills a component. Reflection gives exactly the canonical identifications. □

The phasor edges are obtained by applying the same outward blocks to

$$\left(\frac{h}{\sqrt{3h-2}}, \frac{h}{\sqrt{3h-2}}, h\right), \qquad 1 \leq h \leq 2. \tag{16}$$

This symmetric arc joins $(1, 1, 1)$ to $(1, 1, 2)$. Its other host is $2h/(3h-2)$, and both possible terminal fits have phase $1/2$. Its endpoints satisfy the bounds used in the proposition, so the outward blocks

preserve that phase. The displayed phasors consequently arise from the descent itself, rather than interpolation between integer nodes.

3.5. **Degree and the exact Farey dictionary.** Attach endpoint count vectors $u = (1, 0)$ and $v = (0, 1)$ to the seed. Under an index k update them by

$$(u, v) \longmapsto \begin{cases} ((k-1)(u+v)+v,\ k(u+v)+v), & k > 0, \\ (|k|(u+v)+u,\ (|k|-1)(u+v)+u), & k < 0. \end{cases} \tag{17}$$

Write their sum as (r, s). Their determinant remains ± 1 and their unordered residues modulo two remain $\{(1, 0), (0, 1)\}$. Thus r, s are positive coprime odd integers. Canonical orientation gives $r \le s$. The *Meridian degree* is $D = r + s$. It is the extreme Laurent exponent in ρ^x, where $\rho = (3 + \sqrt{5})/2$; the degree in ρ^{2x} is $D/2$.

Proposition 3.4 (Helm classification)**.** *Canonical Meridians correspond bijectively to coprime positive odd pairs $r \le s$. Their helm labels are the standard Farey fractions r/s.*

Proof. The endpoint vectors are the two Stern–Brocot parents: their sum is (r, s) and their determinant has absolute value one. Conversely, the parents of an odd/odd pair have opposite coordinate parities. Their componentwise absolute difference is a smaller positive primitive odd/odd pair, except at $(1, 1)$. The difference has one componentwise sign; an opposite sign would give the initial pair. Iteration reaches $(1, 1)$.

To recover the signed indices, put $n_\alpha = (r, s)$ and let α^- remove the leftmost index after 1. Consecutive difference vectors have determinant of absolute value two, so three consecutive vectors satisfy $n = 2c\, n^- + \varepsilon n^{--}$ with $c \ge 1$ and $\varepsilon = \pm 1$. Determinant division gives an integer coefficient, parity makes it even, and decreasing coordinate sums fix its magnitude and sign. At the bottom use $(1, 1), (-1, 1)$; canonical orientation fixes the first index positive. The magnitude is fixed by the ratio of successive degrees, which lies in $[2c, 2c+1)$ or $(2c-1, 2c]$ according to the sign; equality occurs only at the first applied index. Reversing the process gives precisely $n_{1,k,k_m,\dots,k_1} = 2|k| n_\alpha + \operatorname{sgn}(k k_m) n_{\alpha^-}$. For the seed use $k_0 = 1$ and $n_\varnothing = (-1, 1)$, so the first extension has $(r, s) = (2k_1 - 1, 2k_1 + 1)$. This recovers the unique address. Mediant addition identifies the label. □

Lemma 3.5 (Phase dictionary)**.** *For helm (r, s) and degree $D = r + s$, the standard Farey label at phase x is*

x	(p, q)	$p + q$
0	(r, s)	D
1	(r, D)	$D + r$
-1	(s, D)	$D + s$
$n \ge 2$	$(D, (n-1)D + r)$	$nD + r$
$-n \le -2$	$(D, (n-1)D + s)$	$nD + s$.

The negative seed phases are omitted.

Proof. At seed phases $0, 1, n \ge 2$, the endpoint bases are respectively $((1, 0), (0, 1))$, $((1, 1), (0, 1))$, and $((1, n), (1, n-1))$. The count updates are linear, so substitution gives the table; negative phase exchanges the bases. For the inverse, odd/odd p, q give $(r, s, x) = (p, q, 0)$. If q is even, sort $p, q - p$ and choose $+1$ when p is the smaller entry, otherwise -1. If p is even, write $q = tp + u$ with $0 < u < p$; sort $u, p - u$ and choose $+(t + 1)$ or $-(t + 1)$ in the same way. A tie is the seed and uses the nonnegative representative. These formulas recover every mark. □

In particular, degree can be read directly from a reduced label:

$$D = \begin{cases} p+q, & p,q \text{ odd}, \\ q, & q \text{ even}, \\ p, & p \text{ even}. \end{cases} \tag{18}$$

This dictionary connects the Meridian and corridor collision windows below.

4. Meridian residues: modulo 27 and Fibonacci moduli

4.1. **Transferring a seed congruence to every address.** The recurrence for the companions contains no division, but a seed period of the *maximum* need not visibly preserve both companions. The following four-entry record resolves that issue:

$$\mathcal{S} = (A, B, C, H) = (9a^2, 9b^2, 3ab, H).$$

Forward and backward orbit steps and pole reflection are the polynomial maps

$$\begin{aligned} \mathcal{R}(A,B,C,H) &= (B, A + 9H^2B - 18HC, HB - C, H), \\ \mathcal{R}^{-1}(A,B,C,H) &= (B + 9H^2A - 18HC, A, HA - C, H), \\ \mathcal{J}(A,B,C,H) &= (A, B, C, C - H). \end{aligned} \tag{19}$$

For $h(x) = M_1(x)$ the seed record is

$$\mathcal{S}_1(x) = (8h(x) - h(x-1) - 2,\ h(x) + h(x-1) + 2,\ h(x) + 1,\ h(x)).$$

Every congruence preserving two consecutive seed maxima therefore propagates along every signed address.

Theorem 4.1 (Largest modulus with a common phase period)**.** *Every canonical Meridian has phase period T modulo m if and only if*

$$m \mid q(T), \qquad q(T) = 3F_{2T}F_{\gcd(2T,4)} = \begin{cases} 3F_{2T}, & T \text{ odd}, \\ 9F_{2T}, & T \text{ even}. \end{cases} \tag{20}$$

In particular, s is a common period modulo F_{2s}.

Proof. Fibonacci addition and (10) give

$$h(x+T) - h(x) = 3F_{2T}F_{4x+2T}.$$

Fibonacci strong divisibility, $\gcd(F_a, F_b) = F_{\gcd(a,b)}$, follows by the Euclidean algorithm from the addition formula. The gcd of all displayed differences is already the gcd of those at $x = 0, 1$, namely $q(T)$. Thus the seed has period T modulo m exactly when $m \mid q(T)$. The record (19) proves sufficiency at every address; the seed itself proves necessity. □

The theorem specifies a period common to all Meridians. It does not assert that the period is the smallest for each individual sequence. Nor does a large period exclude a scalar residue match at two earlier phases. For powers of three it gives

$$M_\alpha(x + 2 \cdot 3^n) \equiv M_\alpha(x) \pmod{3^{n+3}}, \qquad n \geq 0. \tag{21}$$

Indeed, $F_{3j} = F_j(5F_j^2 + 3)$ for even j, beginning with $F_4 = 3$, gives $v_3(F_{4\cdot 3^n}) = n + 1$. Figure 7 shows the common periods at the requested even-indexed Fibonacci moduli.

x	M1							M1.1							M1.2							M1.1.1							M1.-1.1						
s	2	3	4	5	6	7	8	2	3	4	5	6	7	8	2	3	4	5	6	7	8	2	3	4	5	6	7	8	2	3	4	5	6	7	8
F_{2s}	3	8	21	55	144	377	987	3	8	21	55	144	377	987	3	8	21	55	144	377	987	3	8	21	55	144	377	987	3	8	21	55	144	377	987
-12								1	5	13	31	13	231	181	1	1	13	50	1	88	937	2	1	20	50	17	328	944	2	1	5	9	89	285	215
-11								1	2	13	4	34	283	559	1	1	1	46	73	21	715	2	1	2	13	89	94	170	2	1	2	21	89	333	107
-10								1	1	19	13	121	248	544	1	2	16	48	82	270	541	2	2	20	37	98	29	482	2	5	8	34	53	272	869
-9								1	5	1	34	61	57	169	1	1	13	26	1	291	160	2	1	2	51	89	343	653	2	1	8	13	17	241	806
-8								1	2	13	50	130	169	13	1	1	13	53	73	343	433	2	1	20	31	17	34	923	2	1	5	21	17	86	89
-7								1	1	13	31	25	13	34	1	2	1	50	82	56	652	2	2	2	50	98	258	317	2	5	2	9	125	89	233
-6								1	5	19	4	13	34	985	1	1	16	46	1	21	541	2	1	20	13	17	369	104	2	1	8	21	89	233	890
-5								1	2	1	13	34	231	820	1	1	13	48	73	88	580	2	1	2	37	89	328	758	2	1	8	34	89	285	71
-4								1	1	13	34	121	283	181	1	2	13	26	82	21	937	2	2	20	51	98	94	944	2	5	5	13	53	333	215
-3								1	5	13	50	61	248	559	1	1	1	53	1	270	715	2	1	2	31	89	29	170	2	1	2	21	17	272	107
-2								1	2	19	31	130	57	544	1	1	16	50	73	291	541	2	1	20	50	17	343	482	2	1	8	9	17	241	869
-1								1	1	1	4	25	169	169	1	2	13	46	82	343	160	2	2	2	13	98	34	653	2	5	8	21	125	86	806
0	2	2	2	2	2	2	2	1	5	13	13	13	13	13	1	1	13	48	1	56	433	2	1	20	37	17	258	923	2	1	5	34	89	89	89
1	2	5	5	5	5	5	5	1	2	13	34	34	34	34	1	1	1	26	73	21	652	2	1	2	51	89	369	317	2	1	2	13	89	233	233
2	2	5	8	29	29	29	29	1	1	19	50	121	231	985	1	2	16	53	82	88	541	2	2	20	31	98	328	104	2	5	8	21	53	285	890
3	2	2	5	29	50	194	194	1	5	1	31	61	283	820	1	1	13	50	1	21	580	2	1	2	50	89	94	758	2	1	8	9	17	333	71
4	2	5	2	5	29	194	338	1	2	13	4	130	248	181	1	1	13	46	73	270	937	2	1	20	13	17	29	944	2	1	5	21	17	272	215
5	2	5	5	2	5	29	194	1	1	13	13	25	57	559	1	2	1	48	82	291	715	2	2	2	37	98	343	170	2	5	2	34	125	241	107
6	2	2	8	5	2	5	29	1	5	19	34	13	169	544	1	1	16	26	1	343	541	2	1	20	51	17	34	482	2	1	8	13	89	86	869
7	2	5	5	29	5	2	5	1	2	1	50	34	13	169	1	1	13	53	73	56	160	2	1	2	31	89	258	653	2	1	8	21	89	89	806
8	2	5	2	29	29	5	2	1	1	13	31	121	34	13	1	2	13	50	82	21	433	2	2	20	50	98	369	923	2	5	5	9	53	233	89
9	2	2	5	5	50	29	5	1	5	13	4	61	231	34	1	1	1	46	1	88	652	2	1	2	13	89	328	317	2	1	2	21	17	285	233
10	2	5	8	2	29	194	29	1	2	19	13	130	283	985	1	1	16	48	73	21	541	2	1	20	37	17	94	104	2	1	8	34	17	333	890
11	2	5	5	5	5	194	194	1	1	1	34	25	248	820	1	2	13	26	82	270	580	2	2	2	51	98	29	758	2	5	8	13	125	272	71
12	2	2	2	29	2	29	338	1	5	13	50	13	57	181	1	1	13	53	1	291	937	2	1	20	31	17	343	944	2	1	5	21	89	241	215

Figure 7. Five Meridians modulo F_{2s} for $s = 2, \ldots, 8$: the moduli are $3, 8, 21, 55, 144, 377, 987$. Each column has common phase period s, possibly a multiple of an individual least period. The shaded row is the helm; blank cells omit the seed's negative phases. The displayed residues use the reversed Meridian indexing of this edition.

4.2. **Why modulo 27 gives only ten classes.** No positive Markov entry is divisible by three: mutation negates the changed coordinate modulo three and the integral tree starts at $(1,1,1)$. Let t, h be preceding and current poles. An extension by a nonzero index has the particularly simple action

$$S(t,h) = (h,t) \quad (k \text{ even}), \qquad R(t,h) = (h, 7h-t) \quad (k \text{ odd}) \pmod{27}. \tag{22}$$

To see this, put $N_j = 3u_ju_{j+1} - h$. Direct use of the orbit recurrence gives

$$N_0 = t, \quad N_1 = (9u_1^2 - 2)h - t, \quad N_{j+2} - N_j = 9h(u_{j+2}^2 - u_{j+1}^2).$$

All orbit squares are one modulo three, so $N_{j+2} \equiv N_j$ and $N_1 \equiv 7h - t \pmod{27}$. This works for negative indices as well. Only the parity of each recursively applied index survives.

Proposition 4.2 (Universal modulo-27 classes)**.** *At integer phases every Meridian alternates between the two residues of one of the following sets, allowing the two singleton cases:*

$$\{1\},\ \{2,5\},\ \{4,16\},\ \{7,13\},\ \{8,17\},\ \{10,19\},\ \{11,23\},\ \{14,20\},\ \{22,25\},\ \{26\}.$$

The ten sets are pairwise disjoint. Meridians in different classes cannot share an integer value, regardless of degree or phase.

Proof. The common phase period is two because $q(2) = 27$. Track preceding and current poles at both phase parities, starting from $(1,2,1,5)$. The simultaneous maps satisfy $S^2 = I$ and $SRS = R^{-1}$. Successive current-pole pairs on the R orbit are

$$\begin{array}{cccccc} (2,5) & (13,7) & (8,17) & (16,4) & (23,11) & (10,19) \\ (20,14) & (22,25) & (26,26) & (25,22) & (14,20) & (19,10) \\ (11,23) & (4,16) & (17,8) & (7,13) & (5,2) & (1,1). \end{array}$$

The preceding pair is the previous pair cyclically, and $b_{j+1} = 7b_j - b_{j-1}$ checks the return in 18 steps. These states and their S images form a closed set of 36 states. Their current-pole images are exactly the ten listed sets. Congruence of integer values would require membership in the same set. □

Table 1. The ten universal classes and their populations among the 519 Meridians of degree at most 100. Only the population column is bounded-degree data.

Residue set	Population	Residue set	Population
$\{1\}$	42	$\{10,19\}$	47
$\{2,5\}$	88	$\{11,23\}$	47
$\{4,16\}$	61	$\{14,20\}$	38
$\{7,13\}$	78	$\{22,25\}$	35
$\{8,17\}$	65	$\{26\}$	18

At that degree bound, the classification leaves 15,215 of the 134,421 pairs for further comparison. Larger Fibonacci moduli and compatible phases, rather than extrapolation from this table, supply the degree-10,000 certificate in Section 8.

5. Fibonacci matrices, six pieces, and ordering proofs

5.1. **From a Farey label to an actual matching count.** A snake graph is a chain of square tiles, each attached to the right of or above the preceding tile. Shared edges are counted once. A perfect matching covers every vertex exactly once. The Markov snake associated with a reduced $0 < p/q < 1$ is built as follows. Take the lower staircase from $(0, 0)$ to (q, p): at each horizontal coordinate j, step right and then up to height $\lfloor pj/q \rfloor$. Write right steps as a and up steps as b. Write this step sequence as $w_{p/q} = azb$. Remove its first and last letters; start with one square and replace each a of z by two added squares to the right and each b by two upward. The resulting snake has $2(p + q) - 3$ tiles.

Write $\mu(w)$ for its number of perfect matchings. The established Markov matching correspondence gives

$$\mu(w_{p/q}) = m_{p/q}. \tag{23}$$

The matching interpretation originated in the REACH work of 2002–2003. Musiker's memorandum, dated 27 June 2002, proposed the recursive graph model [17]; Itsara, Musiker, Propp, and Viana's manuscript of 10 January 2003 stated and proved the snake-matching correspondence [18, Theorem 3.1]. Setting all edge weights to one gives the ordinary perfect-matching counts. Propp's later exposition, first posted in 2005, records the broader collaborative development [19]. These original contributions precede the later proofs of Aigner's orderings.

For a modern treatment and the Farey-indexed construction, see [16, Section 4.1, Theorem 4.2] and [10]. For example, $w_{2/5} = a^3ba^2b$, its trimmed word is $aabaa$, and the eleven-tile snake has 194 matchings. Auxiliary rearranged words also specify snakes, counted by μ; they need not be canonical Markov snakes.

5.2. **Six pieces and two connector states.** Figure 8 fixes the five three-tile pieces and the three one-square variants of type 6. In a cut between pieces, a matching uses both yellow connector edges or neither: the cut leaves an even number of vertices on either side. Denote these states by 1 and 0. At a selected port remove the two vertices already covered by its connector pair. Direct counting within the pieces gives

piece	00	01	10	11
1	5	2	2	1
2	5	3	3	2
3	5	2	3	1
4	5	3	2	1
5	5	2	2	1
6i	2	1	1	1

(24)

The state order is incoming, outgoing. The one-port end squares 6ii and 6iii have counts $(2, 1)$.

For the ordering surgeries, use a fixed one-ended chop: retain tile triples $(1, 2, 3), (5, 6, 7), \ldots$, with tiles $4, 8, \ldots$ providing paired connectors. A one-square remainder occurs exactly when $p + q$ is even and is counted with the closed end piece. For every connector sequence σ, multiply the applicable row entries in (24); then sum over σ, with outer ports closed. Each matching determines one sequence and one internal completion per piece, and gluing reverses the construction. This proves the counting rule, without an independence assumption. Equivalently it is a sum of terms $5^{k(\sigma)}3^{j(\sigma)}2^{\ell(\sigma)}$, where the exponents count factors of the indicated size. For the $2/5$ snake the piece list $2, 1, 2$ gives

$$5^3 + 5 \cdot 2 \cdot 3 + 3 \cdot 2 \cdot 5 + 3^2 = 194.$$

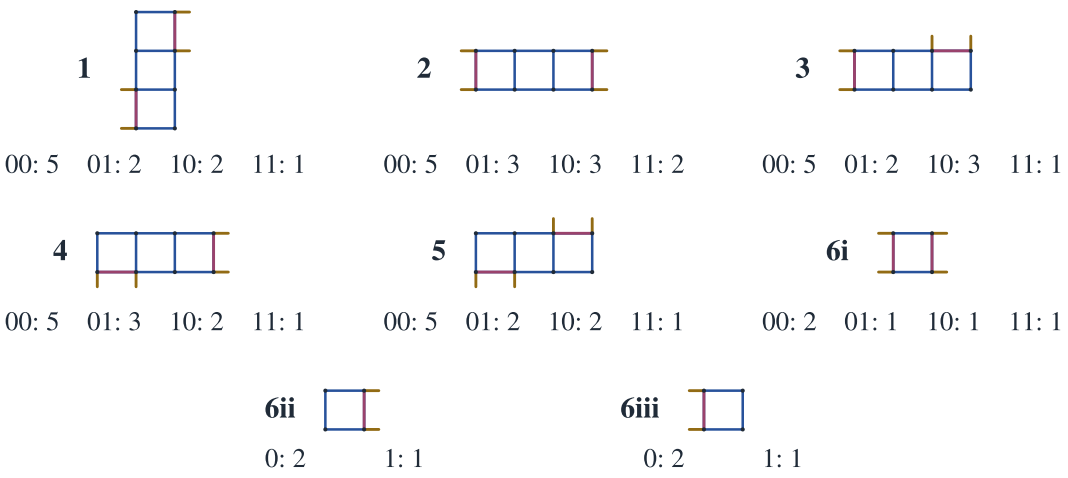


Figure 8. The six physical pieces. Gold edges are paired connectors, magenta marks ports, and dots mark tile vertices. Two-port counts use the order $00, 01, 10, 11$. The central square 6i has counts $(2, 1, 1, 1)$; the one-port end squares have $(2, 1)$. Types 1 and 5 have equal count rows but different physical orientations.

5.3. **Fibonacci-matrix normalization.** The author proposed the Fibonacci-matrix formulation and normalization approach developed here. We begin with the comparison of three consecutive blocks and then apply it to complete products of run blocks.

With $F_0 = 0, F_1 = 1$ and $F_{-j} = (-1)^{j+1}F_j$, the basic odd-index identity is

$$F_{2k-1}F_{2k+3} - F_{2k+1}^2 = 1. \tag{25}$$

For example, $5 \cdot 34 - 13^2 = 1$. Consider the author's three consecutive Fibonacci blocks:

$$\begin{aligned} A &= \begin{pmatrix} F_{2k+3} & F_{2k+1} \\ F_{2k+1} & F_{2k-1} \end{pmatrix}, \\ B &= \begin{pmatrix} F_{2k+1} & F_{2k-1} \\ F_{2k-1} & F_{2k-3} \end{pmatrix}, \\ C &= \begin{pmatrix} F_{2k-1} & F_{2k-3} \\ F_{2k-3} & F_{2k-5} \end{pmatrix}, \qquad k \geq 2. \end{aligned} \tag{26}$$

Applying (25) twice gives precisely the upper-left comparison used in normalization:

$$\begin{aligned} (AC)_{11} - (B^2)_{11} &= (F_{2k+3}F_{2k-1} - F_{2k+1}^2) \\ &\quad + (F_{2k+1}F_{2k-3} - F_{2k-1}^2) = 2. \end{aligned} \tag{27}$$

The same identities in the other entries give

$$AC - B^2 = \begin{pmatrix} 2 & 6 \\ 0 & 2 \end{pmatrix}, \qquad CA - B^2 = \begin{pmatrix} 2 & 0 \\ 6 & 2 \end{pmatrix}.$$

Thus replacing AC or CA by B^2 decreases the upper-left entry even inside a longer product: the surrounding Fibonacci blocks have nonnegative entries and positive upper-left entries. For $k = 3$ this reads $(AC)_{11} = 34 \cdot 5 + 13 \cdot 2 = 196 > 194 = 13^2 + 5^2 = (B^2)_{11}$.

5.3.1. *Run counts and general index shifts.* To apply the same comparison at arbitrary run lengths, index the blocks by

$$\mathcal{A}_t = \begin{pmatrix} F_{2t+3} & F_{2t+1} \\ F_{2t+1} & F_{2t-1} \end{pmatrix}, \qquad t \geq 0. \tag{28}$$

Thus $A = \mathcal{A}_k$, $B = \mathcal{A}_{k-1}$ and $C = \mathcal{A}_{k-2}$ in (26). The four boundary counts of a straight block of $2t+1$ tiles are $F_{2t+3}, F_{2t+1}, F_{2t+1}, F_{2t-1}$: these follow by conditioning on the first edge of a ladder, giving the Fibonacci recurrence; at $t = 0$ they are $(2, 1, 1, 1)$. Gluing successive runs with their paired connector states therefore gives, for $w = a^{h_1}b \cdots a^{h_p}b$ with $h_1 \geq 1$ and $h_j \geq 0$,

$$\mu(w) = [\mathcal{A}_{h_1-1}\mathcal{A}_{h_2} \cdots \mathcal{A}_{h_p}]_{11}. \tag{29}$$

The first run is shortened by the removed initial a; the final b closes the other end. Equivalently, a block-index list $(t_1, \ldots, t_p)$ represents $w = a^{t_1+1}ba^{t_2}b \cdots a^{t_p}b$, with $t_1 + \cdots + t_p = q - 1$.

Fibonacci addition gives the scalar index-shifting identity

$$F_{2r+1}F_{2s+1} - F_{2r-1}F_{2s+3} = F_{2(r-s)-2}.$$

Apply it to the two summands of each product entry to obtain

$$\mathcal{A}_r\mathcal{A}_s - \mathcal{A}_{r-1}\mathcal{A}_{s+1} = 2\begin{pmatrix} F_{2(r-s)-2} & F_{2(r-s)} \\ F_{2(r-s)-4} & F_{2(r-s)-2} \end{pmatrix}, \quad r \geq 1,\ s \geq 0. \tag{30}$$

Consequently, whenever two adjacent indices differ by at least two, moving one unit from the larger to the smaller strictly decreases the whole product's upper-left entry. The case $r = s + 2$ is exactly (27). The only remaining local comparison has adjacent indices differing by one; it is an interchange of the two blocks.

5.3.2. *Comparing the surrounding Fibonacci blocks.* For a finite list of block indices, define the ratio of its two open counts by

$$\rho(u_1, \ldots, u_m) = \frac{[\mathcal{A}_{u_1} \cdots \mathcal{A}_{u_m}]_{21}}{[\mathcal{A}_{u_1} \cdots \mathcal{A}_{u_m}]_{11}}, \qquad \rho(\varnothing) = 0.$$

All these ratios lie in $[0, 1)$. Direct multiplication gives

$$\rho(t, U) = \frac{F_{2t+1} + F_{2t-1}\rho(U)}{F_{2t+3} + F_{2t+1}\rho(U)}. \tag{31}$$

Its right-hand side increases strictly with $\rho(U)$, since (25) gives $\det \mathcal{A}_t = 1$. Moreover, another application of that identity gives

$$\frac{F_{2t+1}}{F_{2t+3}} - \frac{F_{2t+3} + F_{2t+1}}{F_{2t+5} + F_{2t+3}} = \frac{1}{F_{2t+3}(F_{2t+5} + F_{2t+3})} > 0.$$

Hence $\rho(t+1, U) < \rho(t, V)$ for any two finite tails U, V. Two lists can therefore be compared by cancelling equal initial indices: at the first unequal pair, the larger index gives the smaller ratio; an exhausted list has the smaller ratio than any nonempty remainder.

For adjacent blocks in positions $j, j+1$, the outward lists are $(t_{j-1}, \ldots, t_1)$ on the left and $(t_{j+2}, \ldots, t_p)$ on the right. At $r = s + 1$, (30) becomes

$$\mathcal{A}_{s+1}\mathcal{A}_s - \mathcal{A}_s\mathcal{A}_{s+1} = 2\begin{pmatrix} 0 & 1 \\ -1 & 0 \end{pmatrix}.$$

After multiplication by the surrounding blocks, its upper-left entry has the sign of

$$\rho(t_{j+2}, \ldots, t_p) - \rho(t_{j-1}, \ldots, t_1). \tag{32}$$

Indeed, it equals this difference times twice the positive upper-left entries of the two surrounding products. This proves the needed surrounding-block test entirely in the same Fibonacci matrices.

Lemma 5.1 (Fibonacci-matrix normalization)**.** *For coprime positive p, q, every word $w = azb$ with q letters a and p letters b satisfies $\mu(w_{p/q}) \le \mu(w)$.*

Proof. For $p = 1$ there is only the word $a^q b$. Assume $p > 1$ and use the block-index list in (29). Its prefix discrepancies are

$$\delta_j = qj - p(1 + t_1 + \cdots + t_j) \quad (1 \le j \le p), \qquad \delta_0 = \delta_p = 0.$$

Changing (t_j, t_{j+1}) to $(t_j + 1, t_{j+1} - 1)$ decreases only δ_j, by p; the reverse change increases only δ_j, by p. We show that an appropriate change always decreases the matching count until $-p \le \delta_j \le 0$ for every j.

The sign checks use just a prefix-sum identity. Put $h_1 = t_1 + 1$ and $h_i = t_i$ for $i > 1$, the actual run lengths. Whenever $j - m \ge 0$ and $j + m \le p$,

$$\delta_{j-m} + \delta_{j+m} = 2\delta_j + p\left(\sum_{i=j-m+1}^{j} h_i - \sum_{i=j+1}^{j+m} h_i\right). \tag{33}$$

In the block indices, the left sum has the extra 1 precisely when it includes t_1.

First remove positive discrepancies. Choose the rightmost largest $\delta_j > 0$ and transfer one unit from t_{j+1} to t_j. Comparison with its two neighboring discrepancies gives $h_j < q/p < h_{j+1}$; coprimality makes these inequalities strict. Thus the transfer is allowed and $t_{j+1} \ge t_j + 1$; for $j = 1$ the gap is at least two. Gaps of at least two are handled by (30).

If $t_{j+1} = t_j + 1$, compare the outward lists. A first unequal pair with the left index larger would make the parenthesis in (33) nonnegative: the central difference is -1, the equal outward indices cancel, and the first unequal difference is at least 1. This contradicts maximality and the choice of the rightmost maximum. If the left list were exhausted first, its extra initial 1 would instead give $\delta_{2j} = 2\delta_j > \delta_j$, again impossible (including simultaneous exhaustion, when $2j = p$). The left outward ratio is therefore strictly larger than the right one. Reversing the interchange in (32) shows that the selected transfer strictly decreases the count. It also decreases $\sum_{j=1}^{p-1} \delta_j$. There are only finitely many nonnegative block-index lists of sum $q - 1$, so this phase ends with all $\delta_j \le 0$.

Then remove discrepancies below $-p$. Choose the leftmost smallest $\delta_j < -p$ and transfer one unit from t_j to t_{j+1}. For $j > 1$, the neighboring comparisons give $h_j > q/p > h_{j+1}$; for $j = 1$, the inequality $\delta_1 < -p$ gives $t_1 > q/p$, while $t_2 < q/p$. Thus $t_j \ge t_{j+1} + 1$ and the transfer is allowed. Again a gap of at least two is settled by (30).

In the gap-one case, a first unequal outward pair with the left index smaller would make the parenthesis in (33) nonpositive, contradicting minimality and the leftmost choice. If that pair reaches t_1, its extra 1 instead gives $\delta_{2j} \le 2\delta_j + p < \delta_j$, the same contradiction. If the right list were exhausted first, the identity would give $\delta_{2j-p} = 2\delta_j + p < \delta_j$. Simultaneous exhaustion would give $\delta_j = -p$. Thus the left outward ratio is strictly smaller than the right one, and (32) proves a strict decrease in count. The changed discrepancy is $\delta_j + p < 0$, so positivity is not reintroduced. This phase increases the bounded sum of discrepancies by p each time and terminates with $-p \le \delta_j \le 0$.

Finally, $\delta_j \equiv qj \pmod p$. For $1 \le j < p$, coprimality leaves exactly one possible value in $[-p, 0]$, forcing

$$1 + t_1 + \cdots + t_j = \left\lceil \frac{jq}{p} \right\rceil.$$

These are precisely the canonical run lengths. Every transfer has decreased the upper-left product entry, proving the assertion. □

For the canonical word, $h_j = \lceil jq/p \rceil - \lceil (j-1)q/p \rceil$. With $k = 1 + \lfloor (q-1)/p \rfloor$, the factors are the author's A, B from (26), and the end factors are B. For example, $m_{3/8} = [BAB]_{11}$ with $k = 3$. A similar normalization result appears in [13, Proposition 21]; the proof above is self-contained in the author's Fibonacci matrices.

5.4. **The three Aigner orderings.** Fixed-numerator monotonicity was proved by Rabideau and Schiffler [16]; all three orderings were proved by LPTV, Lee–Li–Rabideau–Schiffler, and McShane [13, 14, 15]. The author's Fibonacci matrices prove normalization and the fixed-numerator ordering. His six pieces prove the remaining fixed-sum comparison and the fixed-denominator ordering, using normalization to return to a canonical Markov snake.

Theorem 5.2 (Established monotonicities)**.** *For $i > 0$, whenever both fractions are reduced and lie in $(0, 1)$,*

$$\begin{aligned} m_{p/q} &> m_{(p+i)/(q-i)} && \textit{(fixed sum)}, \\ m_{p/q} &< m_{p/(q+i)} && \textit{(fixed numerator)}, \\ m_{p/q} &< m_{(p+i)/q} && \textit{(fixed denominator)}. \end{aligned}$$

5.4.1. *Fixed numerator: Fibonacci matrices.*

Proof. Fibonacci recurrence gives, for $t \geq 1$,

$$\mathcal{A}_t - \mathcal{A}_{t-1} = \begin{pmatrix} F_{2t+2} & F_{2t} \\ F_{2t} & F_{2t-2} \end{pmatrix}.$$

All entries are nonnegative and the upper-left is positive. Start with $w_{p/(q+i)}$ and delete i internal letters a, retaining the first. Each deletion changes one factor $\mathcal{A}_t$ to $\mathcal{A}_{t-1}$ with $t \geq 1$. Surrounding factors are positive, so the matching count strictly falls. The resulting word ends at (q, p); normalization gives $m_{p/q} \leq \mu(w_*) < m_{p/(q+i)}$. □

5.4.2. *Fixed sum: six pieces.*

Proof. At the same physical cuts, the changes $2 \to 3$ or 4, then 3 or $4 \to 5$, increase no entry of (24); the changed factors are $3 \to 2$ or $2 \to 1$. Rotation $5 \leftrightarrow 1$ preserves the row. Selecting the changed connector and no others exhibits a strictly smaller positive summand whenever an equal-direction join becomes unequal.

The trimmed canonical word begins and ends with a, contains no bb, and has $q - p - 1$ equal joins, all aa. At its rightmost equal join, interchange a, b strictly to the right. That suffix is alternating, so only the chosen join changes. Exactly one prescribed piece changes by the stated rules, while any rotated pieces keep their rows. Each surgery strictly decreases the count. Odd-numbered operations replace one horizontal step by a vertical step in net; even-numbered operations keep the totals. After $2i$ operations the endpoint is $(q - i, p + i)$. There are enough joins because $p + i < q - i$. For the resulting auxiliary word w_*, normalization gives $m_{(p+i)/(q-i)} \leq \mu(w_*) < m_{p/q}$. A similar tail comparison appears in [13, Proposition 22]; here the comparison is proved using the author's six physical pieces. □

5.4.3. *Fixed denominator: six pieces.*

Proof. For the fixed-denominator comparison, refine the same six-piece chop into single-square pieces of type 6, retaining odd-numbered tiles and using the even tiles as paired connectors. A retained square has counts $(2, 1, 1, 1)$ for opposite ports and $(2, 1, 1, 0)$ for adjacent ports. The zero forbids covering their common corner twice. Summing an intervening state regroups these squares into the original three-tile pieces.

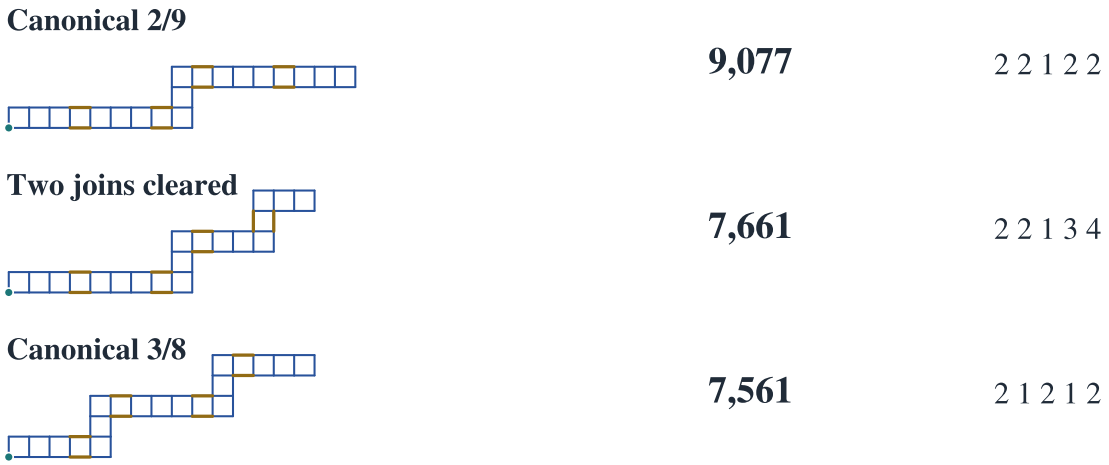


Figure 9. Fixed-sum surgery on the same five pieces. The canonical 2/9 snake has 9077 matchings; after two changes the auxiliary snake has 7661; normalization gives the 3/8 snake with 7561. The intermediate first change, not shown, has 8263. Gold pairs mark cuts and teal dots the starting corners.

Insert one internal b, adding two vertical squares. The affected local counts are the following complete table, with outside ports fixed:

	before				after			
directions	00	01	10	11	00	01	10	11
a, a	2	1	1	1	5	2	2	1
b, b	2	1	1	1	5	3	3	2
a, b	2	1	1	0	5	3	2	1
b, a	2	1	1	0	5	2	3	1

The endpoint caps have the corresponding rows with an outer port closed; the empty trimmed word has the increase $2 \to 5$. No outside count falls, and the all-zero choice witnesses a strict increase. Thus the two added squares compensate for every changed direction.

Starting from $w_{(p+i)/q}$, delete i internal b's and reverse this comparison. At least i are available. Normalizing the resulting word to (q, p) proves $m_{p/q} \le \mu(w_*) < m_{(p+i)/q}$. □

5.5. **Folding an actual snake at its center.** The same local counts also compare families sharing a long initial sequence of pieces. Represent the four counts by

$$R_1 = R_5 = \begin{pmatrix} 5 & 2 \\ 2 & 1 \end{pmatrix}, \quad R_2 = \begin{pmatrix} 5 & 3 \\ 3 & 2 \end{pmatrix}, \quad R_3 = \begin{pmatrix} 5 & 2 \\ 3 & 1 \end{pmatrix}, \quad R_4 = \begin{pmatrix} 5 & 3 \\ 2 & 1 \end{pmatrix}.$$

Attaching piece i to an open-count row (x, y) replaces it by $(x, y)R_i$. This is the sum over the common connector state, not an additional assumption about matchings.

For a helm, use the symmetric central chop: retain the middle square as 6i and group retained squares in pairs outward on each side. For odd/odd p, q, each half has $(p+q-2)/2$ retained squares. If this number is odd, one square remains at each outer end, giving pieces 6ii and 6iii with initial counts $(2, 1)$. Otherwise the half starts at $(1, 0)$ and consists of complete three-tile pieces. This repartition requires rebuilding the piece list; one cannot move a cut and keep its old boundary counts.

Proposition 5.3 (Folded matching counts)**.** *For a reduced $0 < p < q$, let (x, y) be the open counts of one reflected half under the central chop. If p, q are odd, then*

$$m_{p/q} = 2x^2 + 2xy + y^2 = (x + y)^2 + x^2. \tag{34}$$

If $p + q$ is odd, then $m_{p/q} = x^2 + y^2$. In either case $\gcd(x, y) = 1$; a nonempty half has positive counts.

Proof. The trimmed staircase sequence is a palindrome: for $0 < j < q$, $\lfloor p(q-j)/q \rfloor = p - 1 - \lfloor pj/q \rfloor$. For odd/odd labels the two halves meet at an opposite-port central square, whose four counts are $2, 1, 1, 1$. The reflected halves contribute x^2, xy, yx, y^2, giving (34). For opposite parities they meet across a single connector and must use its same state, giving $x^2 + y^2$. Every full piece table and every exposed-square table has determinant ± 1, so its integral inverse preserves the gcd of an open row. Starting at $(1, 0)$ proves primitivity. The first square gives $(2, 1)$, and every subsequent permitted table preserves positivity. □

The seed $1/1$ consists only of its central square. The two examples in Figure 10 give $m_{1/3} = 2 \cdot 2^2 + 2 \cdot 2 \cdot 1 + 1^2 = 13$ and $m_{1/5} = 2 \cdot 5^2 + 2 \cdot 5 \cdot 3 + 3^2 = 89$.

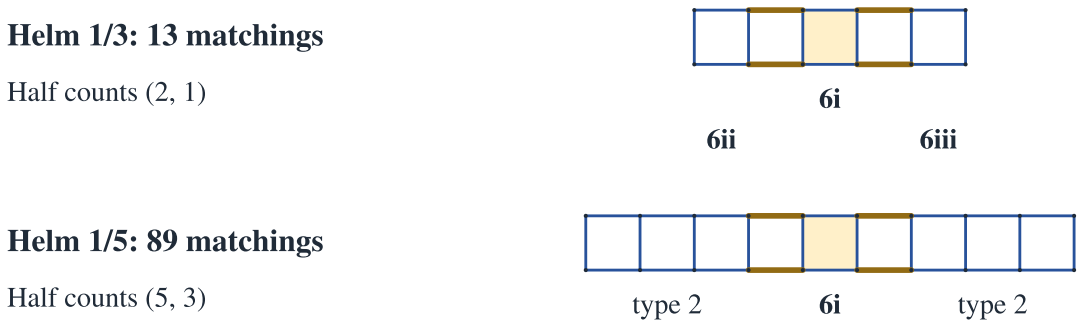


Figure 10. Central and end pieces in actual helms. At $1/3$, central square 6i has the end squares 6ii and 6iii as its halves, with counts $(2, 1)$. At $1/5$, each half is a type-2 triple with counts $(5, 3)$. Folding produces 13 and 89.

5.6. **A common prefix leaves one quadratic comparison.** Two folded graphs with the same outer boundary convention may share a prefix with open counts (x, y). Sum over all remaining states, leaving that cut open. The two centers give positive definite symmetric tables $G, \widetilde{G}$ with determinant one and nonnegative off-diagonal entries. For a helm they have the form SQS^{T} with $Q = \begin{pmatrix} 2 & 1 \\ 1 & 1 \end{pmatrix}$; for opposite-parity labels they have form SS^{T}. Thus

$$m - \widetilde{m} = \alpha x^2 + 2\beta xy + \gamma y^2, \qquad G - \widetilde{G} = \begin{pmatrix} \alpha & \beta \\ \beta & \gamma \end{pmatrix}. \tag{35}$$

Proposition 5.4 (At most one primitive common prefix)**.** *For a nonempty common part and $G \neq \widetilde{G}$, equality requires $\alpha\gamma < 0$ and $\beta^2 - \alpha\gamma$ to be an integer square. There is then at most one primitive positive row (x, y) giving equality. That row must still arise from both actual prescribed snakes.*

Proof. A center table $\begin{pmatrix} a & b \\ b & c \end{pmatrix}$ has $ac - b^2 = 1$ and $b \geq 0$. If its two diagonal differences from another table have the same weak sign, then the difference of $b = \sqrt{ac-1}$ has that sign too. A nonzero difference cannot vanish at a positive row. Opposite diagonal signs are therefore necessary. The resulting quadratic in y/x has one positive root. An integer zero obeys $(\gamma y + \beta x)^2 = (\beta^2 - \alpha\gamma)x^2$; a rational square root of an integer is integral. A positive rational root has only one primitive positive representative. □

For an empty prefix, test its actual boundary row. If $G = \widetilde{G}$, the criterion supplies no exclusion. Equal count tables do not certify equal physical graphs: types 1 and 5 already show why orientations and the prescribed sequence of horizontal and vertical steps must be retained.

A useful uniform exclusion follows directly modulo three. The physical piece tables satisfy $R_i Q R_i^{\mathsf{T}} \equiv Q \pmod 3$, whereas a single retained square gives $-Q$. A helm tail with d retained squares therefore has center table $(-1)^d Q \pmod 3$. Opposite parities give a nonzero difference at every primitive row because the discriminant of Q is -1, a nonsquare modulo three. For equal parity and nonzero difference, let $h = \min_{i,j} v_3((G - \widetilde{G})_{ij})$ and write $3^{-h}(G - \widetilde{G}) = \begin{pmatrix} \alpha & \beta \\ \beta & \gamma \end{pmatrix}$. Then $h \geq 1$. Expanding the equal determinants and reducing modulo three gives $\gamma \equiv \alpha + \beta$; the normalized discriminant is one or two modulo three. If it is two, every primitive shared row has count difference of valuation exactly h. These are exclusions for specified tails with arbitrary actual common prefixes, not a classification of all possible snake-graph collisions.

6. Equal-degree separation and unequal-degree windows

6.1. **A complete result at each fixed degree.** We first use the established fixed-sum, fixed-numerator and fixed-denominator orderings of Markov numbers. Section 5 proves them by matching counts and records their earlier sources.

Theorem 6.1 (Equal-degree unicity)**.** *Distinct canonical integer-phase marks of the same Meridian degree have different maxima. The marks may belong to the same or to different Meridians.*

Proof. For $D \geq 4$, Lemma 3.5 partitions the labels into three classes. Helms r/s have fixed sum D; near-helms $r/D, s/D$ have fixed denominator D; outer phases have fixed numerator D. Each class is strictly ordered by its corresponding monotonicity, and the dictionary ensures that different marks have different labels.

The largest helm is $m_{1/(D-1)}$. The near-helm extrema are $m_{1/D}, m_{(D-1)/D}$; the smallest outer value is $m_{D/(D+1)}$. They are separated by

$$m_{1/(D-1)} < m_{1/D}, \qquad m_{(D-1)/D} < m_{(D-1)/(D+1)} < m_{D/(D+1)}.$$

The intermediate fraction is reduced because D is even. The first two inequalities hold at fixed numerator and the last at fixed denominator. For $D = 2$, the unique seed gives $2, 5$ and then the increasing family $m_{2/(2n-1)}$ for $n \geq 2$, starting at 29. These values are also distinct. □

Thus the remaining Meridian comparison has unequal degrees. To bound it, we need exact leading terms and an explicit positive remainder.

6.2. **From Fibonacci blocks to a Meridian profile.** The ordering argument above uses the Fibonacci and six-piece comparisons from Section 5. We now use the same run matrices to bound growth. Put $\rho = (3+\sqrt{5})/2$ and $\lambda = \log \rho$. The odd-index Fibonacci formula extends (28) to every real t:

$$\mathcal{A}_t = \frac{1}{\sqrt{5}} \left[\rho^{t-1/2} \begin{pmatrix} \rho^2 & \rho \\ \rho & 1 \end{pmatrix} + \rho^{-t+1/2} \begin{pmatrix} \rho^{-2} & \rho^{-1} \\ \rho^{-1} & 1 \end{pmatrix} \right]. \tag{36}$$

For integer t, its entries are exactly $F_{2t+3}, F_{2t+1}, F_{2t+1}, F_{2t-1}$, including negative odd indices. Each displayed matrix is the outer product of a positive column with itself: respectively $(\rho, 1)^{\mathsf{T}}$ and $(\rho^{-1}, 1)^{\mathsf{T}}$. Thus every choice of terms in a product has a positive contribution to its upper-left entry.

Let the helm counts be (r, s) and $D = r + s$. The phase dictionary and the run-count formula (29) give, for every integer $n \geq 2$,

$$M_\alpha(n) = m_{D/((n-1)D+r)}.$$

The first run index is $n-1$; each later index is $n - 1 + \lceil jr/D \rceil - \lceil (j-1)r/D \rceil$. Consequently the full real profile is

$$M_\alpha(x) = \left[\mathcal{A}_{x-1} \prod_{j=2}^{D} \mathcal{A}_{x-1+\lceil jr/D \rceil - \lceil (j-1)r/D \rceil} \right]_{11}. \tag{37}$$

To justify the extension from integers to reals, observe that both sides are finite Laurent polynomials in ρ^x. For the left side this follows from the seed formula and the polynomial recurrence (11); for the right side it follows from (36). Their difference vanishes at every $x = n \geq 2$. Multiplying by a sufficiently large power of ρ^x gives a polynomial with infinitely many roots, so it is zero. For $M_\alpha(-x)$, replace r by s in the right side of (37); the negative-arm dictionary gives the same argument. For example, the seed has $D = 2, r = s = 1$ and $M_1(x) = [\mathcal{A}_{x-1}^2]_{11}$, giving $2, 5, 29, 194, \ldots$.

Proposition 6.2 (Laurent profile)**.** *For helm counts (r, s), degree $D = r + s$, and $t = (r - s)/2$,*

$$M_\alpha(x) = \sum_{j=-D,-D+2,\ldots,D} c_j \rho^{jx}, \quad c_j \geq 0, \quad c_{\sigma D} = \frac{1}{3}(9/5)^{D/2} \rho^{\sigma t}. \tag{38}$$

The logarithm is strictly convex, and the real profile has one minimum.

Proof. Expand the D Fibonacci factors in (37) using (36). Each factor supplies one power ρ^x or ρ^{-x}, with positive coefficients. This gives the stated exponents and coefficient signs.

The run indices sum to $Dx + r - D - 1$. Selecting the first term in every factor gives the upper-left entry

$$\frac{\rho^{Dx+r-D-1-D/2} \rho^2 (3\rho)^{D-1}}{(\sqrt{5})^D} = \frac{1}{3}(9/5)^{D/2} \rho^{Dx+(r-s)/2},$$

because $\rho^2 + 1 = 3\rho$. Selecting every second term gives the other extreme coefficient. The second derivative of the logarithm is λ^2 times the variance of the exponents under their positive normalized weights. Both extremes occur, so that variance is positive; they also force growth at both ends. □

Lemma 6.3 (Uniform Fibonacci-block remainder)**.** *For a Meridian of degree D, helm counts (r, s), $n \geq 0$ and $\sigma = \pm 1$,*

$$M_\alpha(\sigma n) = \frac{1}{3}(9/5)^{D/2} \rho^{\sigma(r-s)/2} \rho^{Dn} (1 + \epsilon_{\alpha,\sigma}(n)), \qquad 0 \leq \epsilon_{\alpha,\sigma}(n) \leq (1 + \rho^{1-2n})^D - 1. \tag{39}$$

Proof. Use (37), replacing r by s on the negative arm. Every block index is either $n-1$ or n. Call the first and second outer products in (36) the $+$ and $-$ choices. When two neighboring columns are multiplied, their inner products are

	$+$	$-$
$+$	3ρ	2
$-$	2	$3/\rho$

.

Relative to the all-$+$ choice, a mixed join has factor $2/(3\rho) < \rho^{-1}$, and a $--$ join has factor ρ^{-2}. At either outside boundary a minus choice has factor ρ^{-2}, which is also at most ρ^{-1}. Each selected minus block touches two joins or boundaries. Thus k minus choices reduce these column and boundary factors by at least ρ^{-2k}.

At a block of index t, replacing the scalar coefficient of the plus term by that of the minus term multiplies it by ρ^{1-2t}. Since $t \geq n-1$, the complete relative contribution of any specified k minus choices is at most $\rho^{-2k}(\rho^{3-2n})^k = \rho^{k(1-2n)}$. Sum this bound over all nonempty subsets of the D positions. The binomial theorem gives the displayed remainder bound. □

6.3. **A finite rectangle depending only on the degrees.**

Theorem 6.4 (Unequal-degree collision window)**.** *Let $D_\alpha \neq D_\beta$, and define*

$$m = \frac{|D_\alpha - D_\beta|}{2}, \qquad E = \max(D_\alpha, D_\beta),$$
$$h = \min\{j \in \mathbb{Z}_{\geq 0} : \rho^j \geq E\}, \qquad N = 3m + h + 3, \qquad T = E(N+2).$$

An integer equality $M_\alpha(x) = M_\beta(y)$ requires

$$|x| \leq \left\lceil \frac{T}{D_\alpha} \right\rceil, \qquad |y| \leq \left\lceil \frac{T}{D_\beta} \right\rceil, \qquad M_\alpha(x) < \rho^T/3. \tag{40}$$

The seed still uses only nonnegative phases.

Proof. The degrees are even, so m is a positive integer. First,

$$|m\log(9/5) - j\log\rho| > \frac{1}{81^m + 1} \qquad (j \in \mathbb{Z}). \tag{41}$$

Choose $j_0 \geq 0$ with $1 < (9/5)^m\rho^{-j_0} < \rho$; equality at an endpoint is impossible by taking the field norm. The positive algebraic integers $9^m - 5^m\rho^{j_0}$ and $5^m\rho^{j_0+1} - 9^m$ have nonzero integer norms and conjugates of absolute value below 9^m. Each is therefore greater than 9^{-m}. Dividing by the appropriate positive denominators makes both adjacent multiplicative gaps greater than 81^{-m}. The inequality $\log(1+u) > u/(1+u)$ gives (41); all other integers j are farther away.

At phases $x = \sigma n$, $y = \tau n'$, the leading logarithms differ by

$$\frac{D_\alpha - D_\beta}{2}\log(9/5) + (D_\alpha n - D_\beta n' + \sigma t_\alpha - \tau t_\beta)\log\rho.$$

The coefficient of $\log\rho$ is integral. Put $r_m = (81^m + 1)^{-1}$. Since $E \leq \rho^h$, $\rho^6 > 81$ and $\rho^5 > 5$,

$$E\rho^{1-2N} \leq \rho^{-6m-5} < \frac{1}{2\cdot 81^m + 3} = \frac{r_m}{r_m + 2}.$$

For a positive integer g and $u \geq 0$ with $gu < 1$, the elementary bound $(1+u)^g \leq \sum_{j\geq 0}(gu)^j = (1-gu)^{-1}$ makes each relative remainder in Lemma 6.3 smaller than $r_m/2$ when its phase magnitude is at least N. Their logarithmic corrections cannot cancel (41). At least one collision phase therefore has magnitude less than N.

The leading coefficient of M_α lies strictly between $\rho^{-D_\alpha}/3$ and $\rho^{D_\alpha}/3$: use $|t_\alpha| < D_\alpha/2$ and $1 < 3/\sqrt{5} < \sqrt{\rho}$ in (38). Lemma 6.3, with $1 + \rho^{1-2N} < \rho$, gives

$$M_\alpha(\pm N) < \rho^{D_\alpha(N+2)}/3 \le \rho^T/3.$$

The same bound holds for M_β. Convexity bounds the value at any phase inside either finite strip by its endpoint values, so the common value is below $\rho^T/3$. Positivity also gives $M_\alpha(\sigma n) > \rho^{D_\alpha(n-1)}/3$ and the corresponding bound for $M_\beta(\tau n')$. Comparing the upper and lower bounds yields $n < 1 + T/D_\alpha$ and $n' < 1 + T/D_\beta$, hence the integer ceilings in (40). □

This theorem bounds the remaining candidates; it does not assert that any candidate collides. It also does not bound the degrees of a hypothetical collision. The next section supplies a different finite reduction, expressed in Farey numerators and denominators rather than Meridian phases.

7. Corridor walls and numerator–denominator windows

7.1. **A second way to travel through the same tree.** The corridor observation groups the walls between neighboring phasors. After an initial entrance, a wall follows a fixed-numerator family

$$m_{p/(q_0+np)}, \qquad n \ge 0.$$

Both Meridian and phasor edges occur in such a route. Their common law is the advance $q \mapsto q + p$, not a rule that distinguishes the two edge colors. For the $5 \to 13$ phasor-capped corridor (equivalently, the $1/2 \to 1/3$ phasor-capped corridor), the fixed-numerator portions are $3/(4 + 3n)$ and $3/(5 + 3n)$, tending to the historical coordinate $c = 1/3$. The first wall begins

$$169 \xrightarrow{\text{phasor}} 2897 \xrightarrow{\text{Meridian}} 51641 \xrightarrow{\text{phasor}} 925765 \longrightarrow \cdots,$$

and the other begins $433, 7561, 135137, 2423525, \ldots$ with the opposite edge alternation.

Corridor role and edge color must be kept separate. With corridor-wall travel designated *standard* and a new entrance *exotic*, the two entry routes here are

$$5 \xrightarrow{\text{exotic}} 29 \xrightarrow{\text{standard}} 433 \xrightarrow{\text{standard}} 7561 \longrightarrow \cdots, \qquad 13 \xrightarrow{\text{exotic}} 169 \xrightarrow{\text{standard}} 2897 \longrightarrow \cdots.$$

Both exotic entrances are Meridian edges. In the first route the initial standard step $29 \to 433$ changes the numerator from two to three; the fixed-numerator formula starts at 433. Thus excluding the concave ceiling arc from a wall's recurrence does not move the exotic entrance to that arc. The graph and its actual depth (14) are unchanged.

7.2. **The exact recurrence behind the observed regularity.** The same Fibonacci run blocks give the corridor recurrence directly. For a reduced label $0 < p/q < 1$, the successive horizontal run lengths are $\lceil jq/p \rceil - \lceil (j-1)q/p \rceil$. Equation (29) therefore reads

$$m_{p/q} = \left[\mathcal{A}_{\lceil q/p \rceil - 1} \prod_{j=2}^{p} \mathcal{A}_{\lceil jq/p \rceil - \lceil (j-1)q/p \rceil} \right]_{11}. \tag{42}$$

The shortened first run is the boundary convention already used for the six-piece matching count. For example, $m_{3/4} = [\mathcal{A}_1^3]_{11} = 169$ and $m_{3/7} = [\mathcal{A}_2^3]_{11} = 2897$.

Replacing q by $q_0 + np$ adds exactly n to each of the p block indices. In the positive expansion (36), each plus choice contributes ρ^n and each minus choice contributes ρ^{-n}. Grouping the terms by the number of minus choices gives

$$m_{p/(q_0+np)} = \sum_{j=0}^{p} c_{p,q_0,j} \rho^{(p-2j)n}, \qquad c_{p,q_0,j} > 0. \tag{43}$$

Every mode occurs. The least order of a constant-coefficient recurrence is therefore $p+1$, with characteristic polynomial

$$\prod_{j=0}^{p}(X-\rho^{p-2j}).$$

Pairing conjugate roots shows that its coefficients are integers. For $p=3$ the polynomial is $(X^2-18X+1)(X^2-3X+1)$, so either wall of this corridor satisfies

$$m_{3/(q+12)} = 21m_{3/(q+9)} - 56m_{3/(q+6)} + 21m_{3/(q+3)} - m_{3/q}. \tag{44}$$

This equality holds at every step, for both colors of edge.

The exact regularity is a shared recurrence, not a constant output ratio. The positive spectral sum gives strict log-convexity, hence

$$\log_{10}\frac{m_{p/(q_0+(n+1)p)}}{m_{p/(q_0+np)}} \nearrow p\log_{10}\rho.$$

The small deviation is retained in the collision argument, rather than discarded as an asymptotic error. Figure 11 shows both the geometric walls and that deviation.

7.3. **A positive correction with a uniform bound.** The sum of the block indices in (42) is $q-1$. Selecting every plus term in (36) therefore gives $3^{p-1}\rho^{q+p/2}/(\sqrt{5})^p$ and hence

$$3m_{p/q} = \left(\frac{3}{\sqrt{5}}\right)^p\left(\frac{1+\sqrt{5}}{2}\right)^{2q+p}(1+\varepsilon_{p,q}), \tag{45}$$

where

$$0 < \varepsilon_{p,q} \le \left(1+\rho^{-2\lfloor q/p\rfloor}\right)^p - 1. \tag{46}$$

For $p>1$, coprimality implies that q/p is not an integer. Every block index in (42), including the shortened first one, is at least $\lfloor q/p\rfloor$. The column and boundary comparison in Lemma 6.3 bounds a specified set of k minus choices by $\rho^{-k}(\rho^{-2\lfloor q/p\rfloor})^k$, which is no larger than $(\rho^{-2\lfloor q/p\rfloor})^k$. Summing over all nonempty subsets proves (46). For $p=1$, the single entry $[\mathcal{A}_{q-1}]_{11} = F_{2q+1}$ has relative correction $\rho^{-2q-1} < \rho^{-2q}$, giving the same bound. This estimate is independent of the remainder class of q modulo p.

Along a fixed wall the correction decreases strictly to zero. Consequently its logarithmic deviations telescope exactly:

$$\sum_{k=0}^{n-1}\left[p\log\rho - \log\frac{m_{p/(q+(k+1)p)}}{m_{p/(q+kp)}}\right] = \log\frac{1+\varepsilon_{p,q}}{1+\varepsilon_{p,q+np}}. \tag{47}$$

Thus there is no accumulated error proportional to the path length. For a route changing corridors, subtraction of the endpoint formula still telescopes, but monotone decay is claimed only within a fixed wall.

Theorem 7.1 (Necessary correction gap)**.** *If $p \neq p'$ and $m_{p/q} = m_{p'/q'}$ for reduced labels, then*

$$\frac{|\varepsilon_{p,q} - \varepsilon_{p',q'}|}{1+\min(\varepsilon_{p,q},\varepsilon_{p',q'})} > 9^{-|p-p'|}. \tag{48}$$

Proof. Assume $p > p'$. The ratio of the leading terms is

$$R = \left(\frac{3(1+\sqrt{5})}{2\sqrt{5}}\right)^{p-p'}\rho^{q-q'}.$$

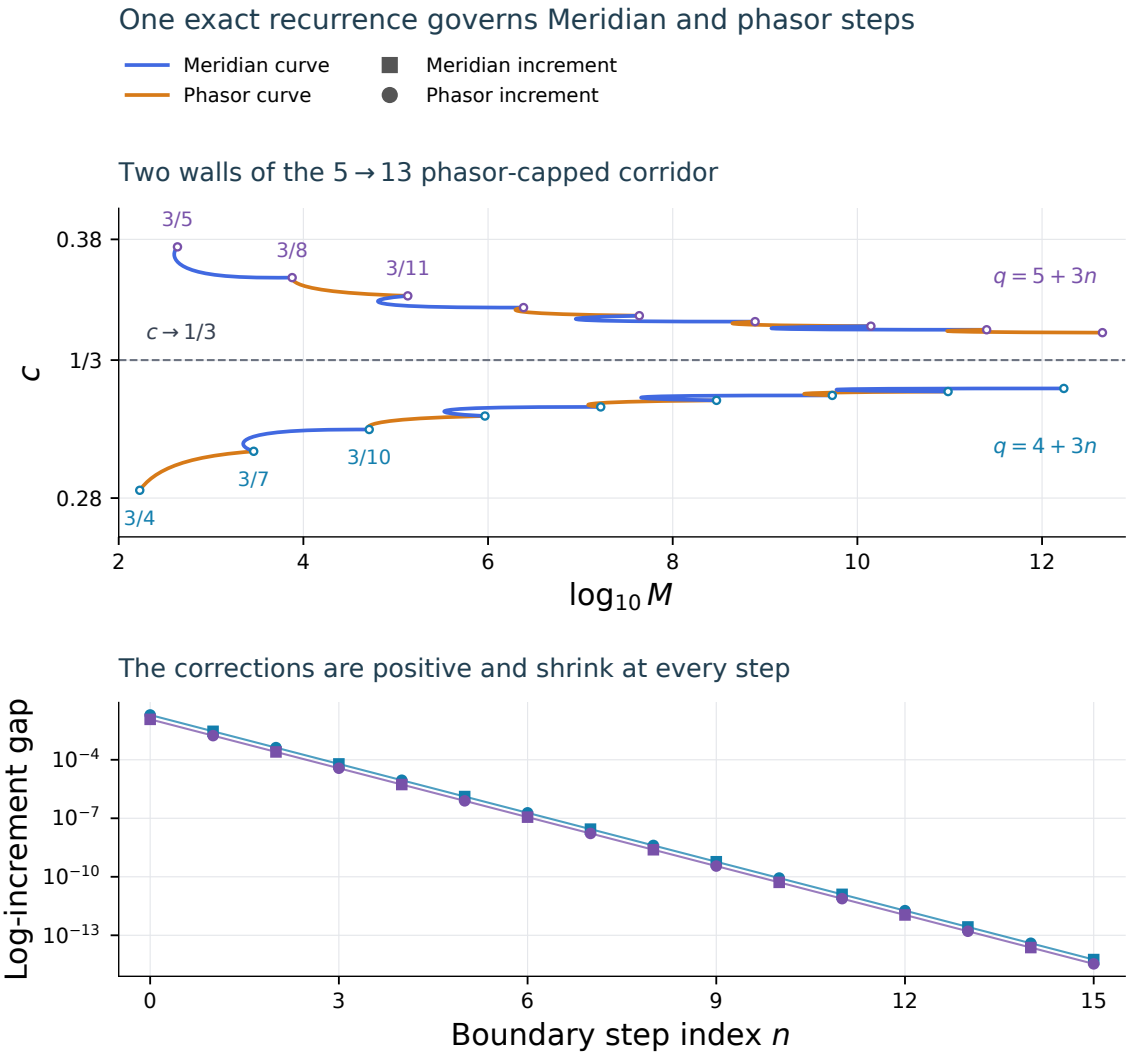


Figure 11. The two fixed-numerator walls of the $5 \to 13$ phasor-capped corridor ($1/2 \to 1/3$ in fraction labels). The concave ceiling arc is omitted from this recurrence illustration. Both walls obey (44). In the lower panel, the positive difference between $3\log_{10}\rho$ and the actual logarithmic increment decreases at every step. Squares denote Meridian increments and circles phasor increments. The values are exact integers; only the plotted curves and logarithms are numerical.

Its quadratic-field norm is $(9/5)^{p-p'}$, so $R \neq 1$. The number $(\sqrt{5})^{p-p'}(R-1)$ is an algebraic integer, because the powers of $(1+\sqrt{5})/2$ and ρ are units. Its nonzero norm gives

$$|(R-1)(\overline{R}-1)| \geq 5^{-(p-p')}, \qquad \overline{R} = (9/5)^{p-p'}/R > 0.$$

Put $\eta = \max(R, R^{-1}) - 1$. If $R \geq 1$, then $|R-1| = \eta$ and $|\overline{R}-1| < (9/5)^{p-p'}$. If $R < 1$, their product is $\eta((9/5)^{p-p'} - 1/(1+\eta)) < \eta(9/5)^{p-p'}$. Either case forces $\eta > 9^{-(p-p')}$. At equality of the Markov values, $R = (1+\varepsilon_{p',q'})/(1+\varepsilon_{p,q})$, so η is precisely the left side of (48). □

7.4. **The corridor collision window.**

Theorem 7.2 (Numerator–denominator window)**.** *Let $p \neq p'$, $P = \max(p, p')$, and let K be the least nonnegative integer satisfying*

$$\rho^{2K} > P(9^{|p-p'|} + 1). \tag{49}$$

Every equality $m_{p/q} = m_{p'/q'}$ requires

$$\max(q, q') \leq P(K + 1) - 1. \tag{50}$$

For bounded numerators a simpler, weaker consequence is $\max(q, q') \leq 2P^2 + P - 1$.

Proof. If both quotient floors are at least K, then $P\rho^{-2K} < 1/(9^{|p-p'|}+1)$. The elementary estimate $(1 + u)^p \leq (1 - pu)^{-1}$ for $pu < 1$ makes both corrections strictly smaller than $9^{-|p-p'|}$, contradicting Theorem 7.1. Thus one denominator, say q, is at most $Kp - 1$.

The Fibonacci formula (36) gives the entrywise bound $\mathcal{A}_t \leq \rho^t \mathcal{A}_0$ for every integer $t \geq 0$. Products preserve that bound, and $\mathcal{A}_0 = \begin{pmatrix} 2 & 1 \\ 1 & 1 \end{pmatrix}$ has operator norm ρ. Since the indices sum to $q - 1$, (42) gives $m_{p/q} \leq \rho^{q-1}[\mathcal{A}_0^p]_{11} \leq \rho^{q+p-1}$. Together with the positive leading term, this yields

$$\frac{1}{3}\rho^{q'} < m_{p'/q'} = m_{p/q} \leq \rho^{q+p-1}.$$

Now $3 < \rho^2$ implies $q' < q + p + 1$. The denominators are integers, so $q' \leq q + p$. It follows that both denominators are at most $P(K + 1) - 1$. For the simpler bound it suffices to use $K = 2P$: $\rho^{4P} > 36^P > P(9^{P-1} + 1)$ for $P \geq 2$, and $|p - p'| \leq P - 1$. □

For example, numerators at most 64 permit $K = 75$, so every remaining comparison lies at denominators at most 4863. With $P = 64$ and numerator difference five, $K = 8$ gives 575. These are bounds on candidates, not new numerical verification claims.

Theorem 6.1 first discards equal Meridian degrees. For the rest, the phase rectangle (40) and denominator cap (50) can be imposed together through the dictionary (18). Fixed-numerator ordering already separates all labels with $p = p'$. What remains is a comparison of different numerators and degrees inside their joint windows. Neither numerator nor degree is globally bounded by these theorems, so this is not yet a finite reduction of the entire unicity conjecture.

8. All-phase verification through degree 10,000

Theorem 8.1 (Degree-10,000 separation)**.** *Among canonical Meridians of Laurent degree at most* 10,000*, distinct canonical integer-phase marks have distinct maxima. There are exactly* 5,067,077 *Meridians in this family.*

The computational part separates different Meridians at all integer phases. The fixed-degree theorem also separates marks on a single Meridian, so the two conclusions combine as stated. The bound is on *degree*, not on the size of a Markov number, and it does not exclude a competitor of higher degree.

8.1. **Why a finite residue test covers infinitely many phases.** For a period T, define the complete image

$$\mathcal{R}_\alpha(T) = \{M_\alpha(x) \bmod q(T) : 0 \leq x < T\}.$$

Theorem 4.1 makes this the image at *every* integer phase. Disjoint images therefore separate two entire Meridians. If images overlap for several periods, a true equality must use compatible phases in all of them. Define the witness relation

$$W_T(\alpha, \beta) = \{(u, v) \in (\mathbb{Z}/T\mathbb{Z})^2 : M_\alpha(u) \equiv M_\beta(v) \pmod{q(T)}\}.$$

Proposition 8.2 (Compatible witnesses)**.** *Equality of two integer values requires one witness in each selected W_T, with first coordinates agreeing modulo every pairwise gcd of the periods, and second coordinates agreeing in the same way. If no compatible choice exists, the two Meridians are disjoint at all integer phases.*

Proof. A true equality uses the same integers x, y in every modulus and hence supplies the required residues. Conversely, the generalized Chinese remainder theorem lifts compatible coordinates to a phase pair modulo the least common multiple. This converse concerns modular witnesses only; it does not imply equality of the full values. □

The moduli need not be independent. In particular, the periods $36, 38, 40$ are all even, so contradictory parity requirements alone can exclude a pair that survives each separate image test.

8.2. **Complete inventory and the final exclusion.**

Proof of Theorem 8.1. Proposition 3.4 identifies the inventory with coprime positive odd pairs $r \le s$, $r + s \le 10{,}000$. It contains 5,067,077 Meridians and 12,837,632,128,426 unordered pairs. The producer enumerates the count-vector address tree; an independent checker enumerates the coprime pairs directly and compares the inventories. The child degree is $2|k|D \pm (|v| - |u|) > D$, where $|u|, |v|$ are the endpoint word lengths. This gives finite exhaustive index ranges.

Every one of the 36 phase residues of every Meridian is evaluated modulo $q(36)$. Equal-residue grouping lists all pairs whose images intersect; its complement is excluded at once. Periods 38 and 40 are then evaluated on every endpoint of the preceding survivor sets. The complete image tests leave 87 pairs. For each of them, project every full witness relation onto the four parity pairs $(u \bmod 2, v \bmod 2)$. The three projected sets have empty intersection in all 87 cases. Proposition 8.2 therefore excludes every pair of different Meridians at every integer phase. Theorem 6.1 also excludes different marks within each individual Meridian, completing the statement. □

Table 2. Complete cumulative survivor counts from the archived certificates. "Images" forgets meeting phases; "phases" also imposes compatibility. Survivors are modular coincidences, not integer collisions.

Tests retained	$D \le 2{,}000$	$D \le 10{,}000$
36: images	7,121	320,755
36, 38: images	612	17,427
36, 38: phases	2	2,052
36, 38, 40: images	0	87
36, 38, 40: phases	**0**	**0**
36, 38, 40, 42: images	—	1
36, 38, 40, 42, 44: images	—	0

8.3. **What was checked independently.** The degree-10,000 producer uses signed endpoint-orbit updates. The separate evaluator uses Fibonacci staircase words with Euclidean matrix reduction. They agree on all 188,369,412 retained phase evaluations. The checker verifies the 182,414,772 baseline phase tags bijectively, so an omitted or repeated phase record cannot pass unnoticed. Independent sorting of the original unsorted buckets reconstructs all 70,009 cross-Meridian residue groups and the subsequent complete pair sets. Coverage is checked by exact records, not inferred merely from their counts or from a matching digest.

The phase result is checked three ways: full generalized-CRT joins, an independent 16-bit mask computation on $(x \bmod 4, y \bmod 4)$, and the weaker four-state parity projection, already sufficient for the final 87. The degree-2,000 certificate, containing 202,862 Meridians, was completed first; its common survivor sets agree exactly with the larger inventory when identified by helm labels.

Five deliberate corruptions—an altered value, an incorrect modulus, a duplicate tag, an omitted record and an invented pair—were all rejected. The degree-100 control compares 18,684 residues with literal Fibonacci words and the polynomial record of (19). The optional image-only extension through periods 42 and 44 also ends with zero pairs; all 88 period-44 values were separately checked using arbitrary-size Python integers because $q(44) > 2^{63}$.

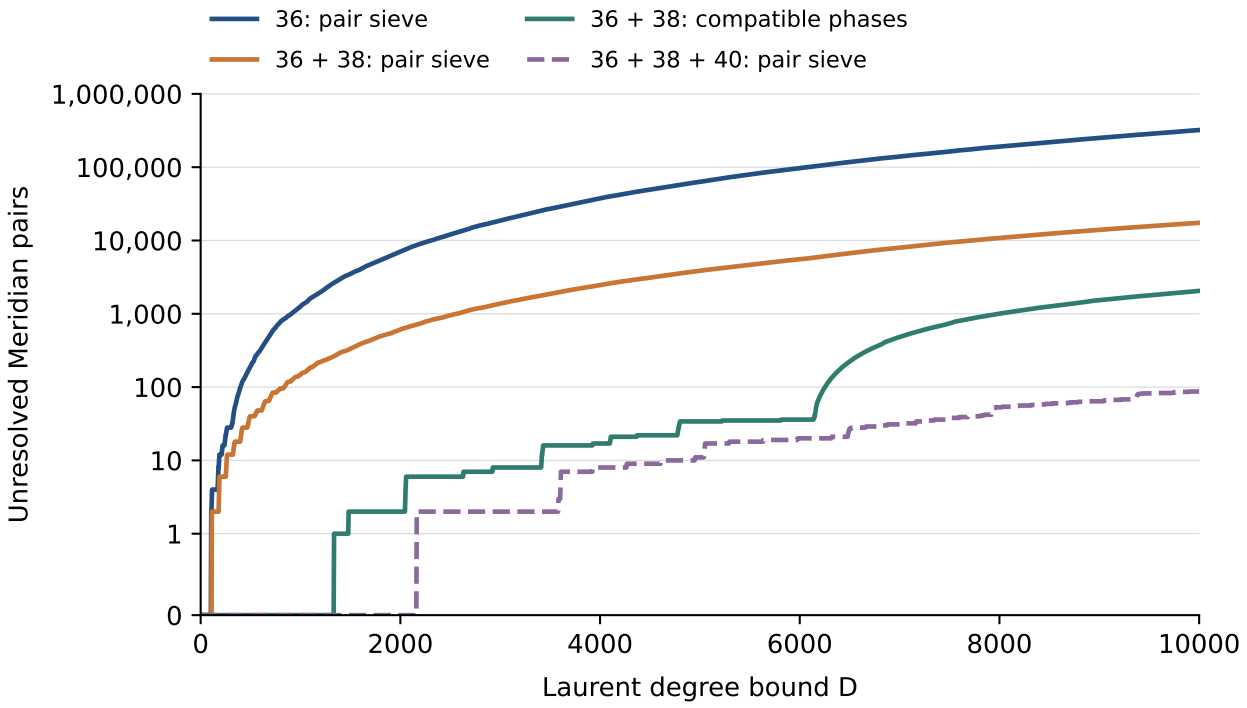


Figure 12. Exact unresolved-pair profiles in the degree-10,000 inventory. The phase-compatible sieve through period 40 has no survivors in the entire displayed range. Lines join discrete even-degree bounds. The figure is a record of the finite certificate, with no extrapolation to larger degrees.

8.4. **Reproducibility and scope.** The degree reproducibility package [11] contains the inventory, compact residue groups, phase witnesses, producer and checker sources, audit receipts, and a regeneration driver. Large baseline tables are regenerated; their recorded sizes and hashes identify the original run. The reindexed edition retains the original computational kernels with an explicit address-convention adapter. Reversing the written address tail does not change a helm label, degree, phase, or certified numerical value.

This is a deterministic computer-assisted certificate, not an external referee report or proof-assistant formalization. Its scope is a bounded set of Meridians with unbounded phase. The numerical-order verification in Section 9 is a separate computation with its own coverage proof and execution record.

9. Fast verification with bounded working storage

9.1. **The completed comparison.** The completed combined run [4] checked **1,101,388,071,945 configurations** and certified that each of the **first one trillion Markov values in numerical order** is the maximum of exactly one normalized triple. These counts answer different questions: the larger is the workload, including possible competitors and conservative cutoff coverage; the smaller is the guaranteed numerical prefix. The exact trillionth value and its predecessor are supplied in full in the selected-values supplement; each has 1,021,609 decimal digits. The title names the certified numerical prefix, not the larger comparison workload.

Meridian analysis guided the organization by scale. A helm anchors a family, and its degree determines the limiting logarithmic spacing along each outward branch. This suggested asking which families can contribute at a given scale, rather than retaining every value already generated. Finite-phase corrections still require certified bounds: the degree and helm alone are not an exact band-entry test.

The production code implements this idea using reduced Farey labels p/q, together with the separate root, and compressed Vieta recurrences. Groups of neighboring Farey directions share certified matrix bounds. They let the code select the addresses relevant to a magnitude band without keeping a separate schedule for every Meridian. The band algorithm can be formulated entirely in these Farey and matrix terms; the Meridian work supplied the family-growth viewpoint that guided its development. The implementation first selects by certified magnitude, then compares eight-byte residues within each band. Full integers are reconstructed only for repeated residues. Completed key files are removed before the next band is processed. Thus the working store depends on the band size rather than the total number of configurations. Its correctness uses exhaustive band coverage and exact residue resolution, without the Meridian collision-exclusion theorems. No controlled comparison isolates a runtime or storage gain attributable to Meridian coordinates alone.

Table 3. Completed comparison and certified numerical coverage. Overlapping band emissions are not counted as new configurations.

Certified numerical-value prefix	1,000,000,000,000
Inner configurations below the cutoff	1,000,000,419,685
Included configurations compared	1,101,388,071,945
Band emissions, including overlap	1,107,352,458,539
Committed bands	19,287
Repeated residue groups / exact members	12 / 24
Equal maxima found	0

9.2. **Coverage and why no collision can cross a cleared band.** The finite envelope uses the same height bounds as the earlier fifty-billion proof [7]. For reduced labels $0 < p \le q$,

$$m_{p/q} \le F_{2(p+q)-1}, \qquad m_{p/q}^2 \ge 4\,5^{p+q-2}.$$

Including the root, the number of configurations of height at most $t \ge 2$ is $C(t) = 1 + \frac{1}{2}\sum_{j=1}^{t} \varphi(j)$, where φ is Euler's totient function. The exact choices are

$$K = 2{,}565{,}100, \qquad B = F_{5,130,199}, \qquad L = 3{,}067{,}794,$$
$$C(K) = 1{,}000{,}000{,}419{,}685, \qquad C(L) = 1{,}430{,}355{,}600{,}632.$$

Every inner configuration has maximum at most B. The exact inequalities $4\,5^{L-2} \le B^2 < 4\,5^{L-1}$ ensure that every competitor with maximum at most B has height at most L. This argument counts configurations before making any claim of unicity.

To schedule the comparisons, 162 cones partition the remaining fraction labels after the 163 configurations through height 32, including the root. Here a *cone* means the addresses strictly between two neighboring Farey labels, after their already retained endpoints are removed. For endpoints $p_L/q_L < p_R/q_R$, each address in the group has the unique form

$$(p, q) = u(p_L, q_L) + v(p_R, q_R), \qquad u, v \ge 1, \quad \gcd(u, v) = 1.$$

The endpoints satisfy $p_R q_L - p_L q_R = 1$. They are obtained by repeatedly inserting mediants until the next numerator-plus-denominator exceeds 32. This is a finite partition of address directions, not a partition into individual Meridians. One Meridian can cross several cones, and one cone can contain parts of many Meridians.

Figure 13 connects the motivating family picture to this implementation. In the group $0/1 < p/q < 1/31$, for example, $(p, q) = (v, u + 31v)$. The displayed positive branches of degrees 2 and 4 eventually lie in the rows $v = 2$ and $v = 4$. Their predictable growth makes selection by scale natural; the shared cone bounds make that selection certified for every address in the group, including other families. Exact positive-matrix bounds assign each label an interval containing $\log(3m_{p/q})$; the coefficients are rounded outward at scale 2^{-32}. The bands cover from zero through a certified upper endpoint beyond $\log(3B)$, without gaps. Every configuration whose interval intersects a band is emitted there, including intervals crossing a boundary. The frozen cone certificate and integer inequalities are checked before use.

If two maxima were equal, their actual logarithms would occupy the same band. Both enclosing intervals would intersect that band, and both exact residues modulo 2^{64} would therefore enter the same comparison. All keys in a band are partitioned into 32 complete buckets and sorted. Every member of every repeated-key group is recovered by replaying the band and is compared exactly. Only then is the band committed and cleared. Consequently, clearing its keys cannot hide an equality across a boundary. Neither random-residue assumptions nor family-specific collision exclusions are used to discharge a repeated group.

All 12 repeated groups contained two configurations. Independent integer evaluators agreed on their values, and every pair had unequal maxima. The complete inner population and the outer envelope therefore establish the first-trillion conclusion in Table 3.

9.3. **Completion timestamp, elapsed work, CPU time, and storage.** The inherited chain began on **8 November 2026 at 14:55:01.580398 UTC** (08:55:01.580398 CST). The extension's first retained band began on **9 November at 16:53:38.951229 UTC** (10:53:38.951229 CST). Its last band finished on **10 November at 03:54:02.997413 UTC**, or **9 November at 21:54:02.997413 CST** in St. Louis. The extension session ran from 16:53:13.152936 UTC on 9 November (10:53:13.152936 CST) through 03:54:13.271944 UTC on 10 November (21:54:13.271944 CST on 9 November). The final independent replay ended at 03:56:16.801036 UTC (21:56:16.801036 CST on 9 November); verification and replay of a fresh portable extraction ended at 03:59:41.149704 UTC (21:59:41.149704 CST on 9 November).

The under-24-hour figure is retained active elapsed processing, including the inherited certificate. It excludes pauses, restoration, failed or lost attempts, and later audits. The combined calendar span exceeds active processing by 46,908.545871 seconds (13.030 hours); this difference includes all such gaps and overhead and is not a measure of idle time alone. The inherited execution record includes 23,436,403,353 configurations regenerated after an environment loss, with 0.827 hours of lost band work recorded separately. The inherited execution windows total 17.160 hours, including known lost work. Three interrupted extension sessions have bounded, rather than exact, end times. The extension execution windows total 35,390.008304–35,547.876597 seconds; 3,617.747371–3,775.615664

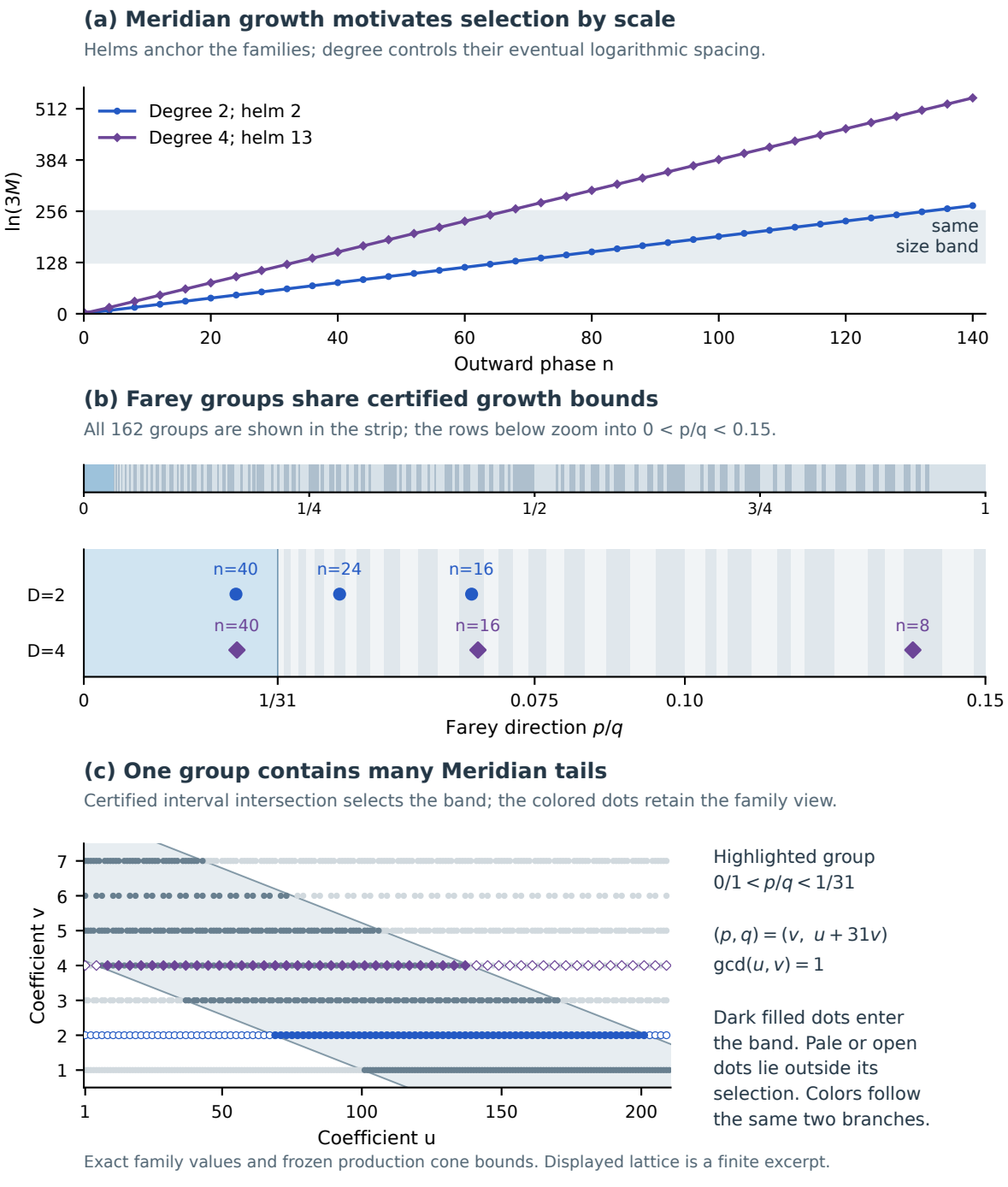


Figure 13. From Meridian growth to certified Farey grouping. (a) Exact values on two positive branches illustrate the degree-dependent spacing that motivated magnitude bands; the shaded band is $128 \le \log(3M) < 256$. (b) All 162 frozen Farey groups, then a zoom showing the same families crossing their boundaries. (c) The highlighted group $0/1 < p/q < 1/31$ uses $(p, q) = (v, u + 31v)$ with positive coprime u, v. Shading selects certified intervals meeting the band in (a); colors pick out the same branches among all displayed addresses. Groups share matrix bounds and can contain many Meridian tails. Boundary-crossing intervals enter both bands. Exact plotted data and the frozen certificate accompany the source.

Table 4. Measured resources for the completed retained chain. The run used eight workers. GiB denotes 2^{30} bytes.

Measurement	Recorded amount
Retained active band processing, combined	86,243.145675 s **23 h 57 min 23.146 s**
Inherited / extension active processing	54,470.884742 / 31,772.260933 s
Summed native-child CPU, combined	417,823.596537 s (116.062 h)
Inherited / extension native-child CPU	264,075.377305 / 153,748.219232 s
Calendar span, first inherited band to final session end	133,151.691546 s (36.987 h)
Extension calendar span, session endpoints	39,660.119008 s (11.017 h)
Maximum recorded temporary key files	**1,065,664,392 bytes** 1,016.297 MiB; 0.992 GiB
Maximum generator resident memory	36,468 KiB (35.613 MiB)
Verified compressed recovery archive	38,920,281 bytes (37.117 MiB)
Independent final replay	67.501145 s
Portable extraction verification and replay	71.627535 s

seconds within those windows are outside retained band time, and 4,112.242411–4,270.110704 seconds fall between windows. These include overhead and interrupted attempts, not only idle time. The final evidence preserves the individual session bounds.

The combined retained stages used 49,481.812969 seconds for generation, 25,077.576696 for partitioning, 11,304.684507 for sorting and scans, and 121.285178 for exact-group resolution; controller bookkeeping accounts for the remaining band time. CPU time sums native-child usage and does not include an independently totalled parent-process CPU measurement.

The storage peak counts logical temporary key files, including a shard temporarily duplicated during partitioning. It excludes receipts, source, backup copies, filesystem overhead, and unrelated work. The generator memory peak covers that native process only. Continuous whole-workspace disk and aggregate-memory peaks were not recorded.

9.4. **Replay and retained evidence.** The final audits checked the frozen sources, all 19,287 linked receipts (13,638 inherited and 5,649 extension), boundaries, counts, bucket accounting and retained candidate bytes. A separate checker recomputed the envelope, independently reconstructed all candidate maxima with polynomial recurrences, and regenerated every repeated-key band. A fresh extraction verified all 20,208 manifested archive members and replayed the same final chain, with no partial or skipped-check flags. This is a receipt-and-candidate replay, not a second generation of every discarded singleton key.

The frozen recovery archive [4] is

`v16_Trillion_Verifier_Recovery.zip`

Its SHA-256 and the final extension receipt head are, respectively,

`6aac7138c8427eb5a3701b27b841e55a75a2e1960c534233261b42375deaeeea`

`624c31904f64f8d9434162396a311228f2ece95d495ff2c7dc9d053314ed0c72`

The source includes the final replay reports, resource reconciliation, statistics and the unchanged historical evidence. Independent here means a separate implementation within the project, not external peer review.

9.5. **Reusing the completed 500-billion certificate.** The earlier certificate [6] completed on 9 November 2026 at 15:50:31.046707 UTC (09:50:31.046707 CST), comparing 550,693,634,649 configurations in 13,638 bands. It certified the first 500 billion values, with four repeated groups, 15 h 07 min 50.885 s of retained active work and a 754,846,136-byte temporary key-file peak. Its unchanged final receipt head is

`4642f18be7adf418d5399ffa87825dc2183dae6808ef7516e0dd0b1d704b9b6d.`

The separate extension adds 550,694,437,296 configurations and 8 h 49 min 32.261 s of retained active work. The enlarged envelope admits no new configuration into an already cleared band: the certified lower endpoint of every newly admitted interval lies beyond the old cutoff. Intervals crossing the join are emitted again. Each address is counted only once, in the band containing its lower interval endpoint. All 550,693,634,649 inherited configurations lie within the new inner height. The exact join proof and both frozen manifests accompany the evidence. Here $C(K-1) = 999{,}999{,}913{,}445$ and $C(K) = 1{,}000{,}000{,}419{,}685$; thus the inner population suffices for the claimed first-trillion prefix.

9.6. **Comparison with Tan–Zhang.** Tan and Zhang [20] report uniqueness for 239,536,376,556 normalized maxima through 10^{500000}, in the computation archived on 26 October 2026. Their 48-bit screening and replay modulo 2^{128} provide a useful recent comparison. The 13-group, 91-job screen processes 3,113,973,008,796 records, including repeated coverage. Our completed trillion-value prefix compares 1,101,388,071,945 configurations in 1,107,352,458,539 band emissions, using 64-bit residues within certified magnitude bands and full-integer resolution of repeats. These larger workload counts are distinct from the numerical-prefix sizes. Both methods use certified size information. Tan–Zhang use it to enforce their common cutoff, then compare balanced subtree groups in all pair jobs. Here the bounds schedule local magnitude bands whose completed keys can be cleared. Figure 14 shows this difference and the Meridian reasoning behind our choice of organization.

Storage and timing must be compared by scope. Tan and Zhang report about 184.27 GB of five-byte payload for the largest pair job and recommend 250 GB of available disk; their original target replay used 16 workers. Our completed run used eight workers and a maximum recorded 1,065,664,392 bytes (1.066 GB; 0.992 GiB) of temporary key files, with 23 h 57 min 23.146 s of retained active processing. Neither payload figure is a measured whole-machine storage peak. Tan and Zhang explain that their interrupted, multi-day run's partial timers do not establish a reliable total runtime, so a wall-clock or CPU speedup ratio is not justified. The comparison uses their cited version 1, still current when checked on 9 November 2026.

9.7. **Selected decimal values and run statistics.** The selected-values supplement supplies the *complete base-10 expansions* of six selected values: the trillionth Markov value and its predecessor (counting 1 first), the last value below and first value above $10^{1000000}$, and the last value below and first value above 10^{999999}. The last of these is the first Markov value with one million decimal digits. Each integer occupies one plain-text file, compressed losslessly in the supplementary ZIP, with its address and checksum. The six files contain 6,043,218 digits in total. The expansions were first posted on Zenodo on 9 November 2026 [5]. The completed unicity certificate and subsequent

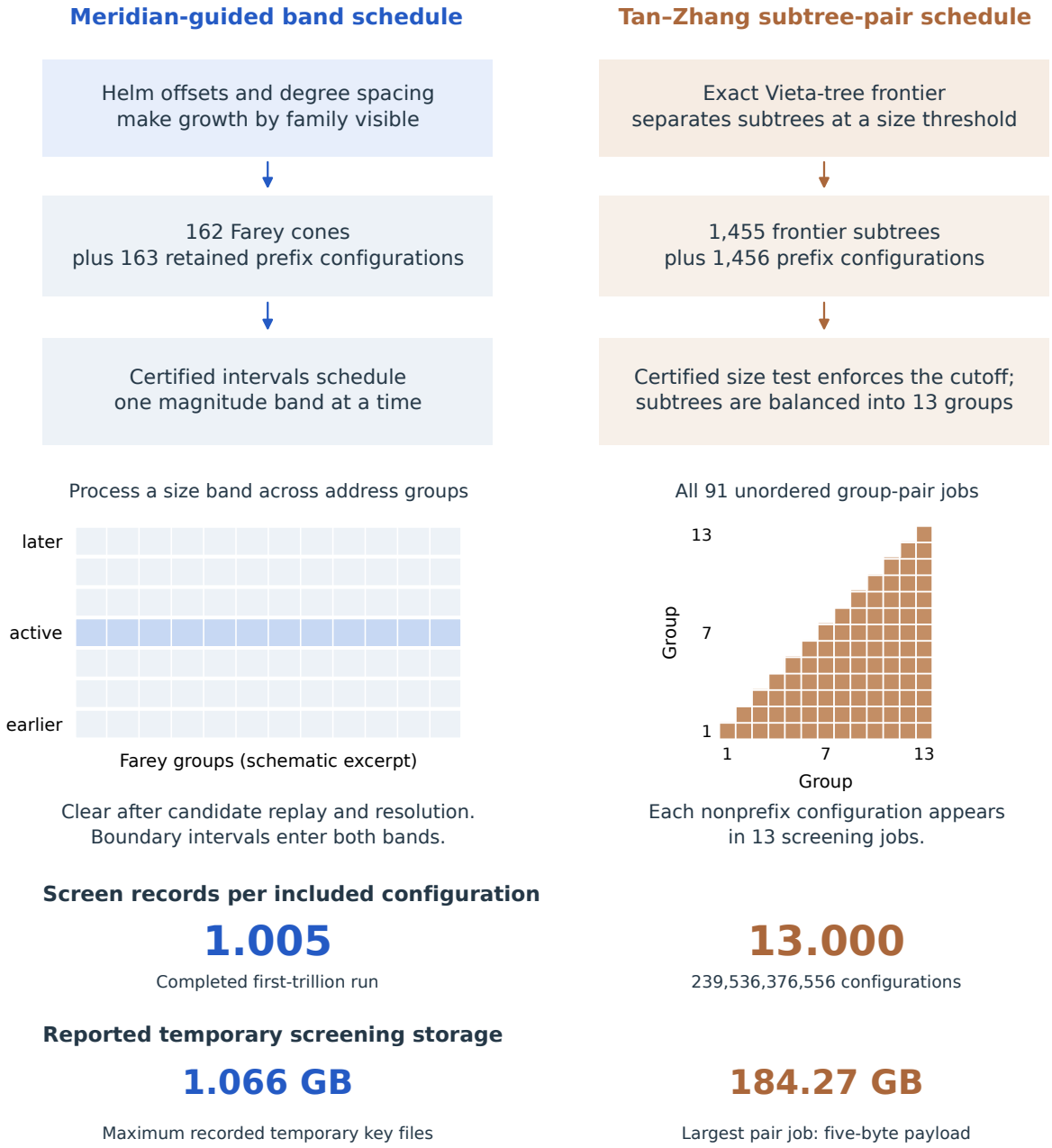


Figure 14. Two organizations of the comparison workload. Diagram geometry is schematic; partition counts and screen totals come from the completed runs. Meridian growth guided our band schedule, implemented with Farey-cone bounds. Tan–Zhang [20] balance their frontier subtrees into 13 groups and screen all 91 unordered group pairs, including diagonals. Their nonprefix configurations enter 13 jobs; our certified boundary overlaps cause some repeat emissions. Ratios count original screening records, excluding candidate replay and audits; they are not CPU speedups. Storage labels state the measured or reported components. Both methods require certified size bounds and modular arithmetic. The comparison does not assert a whole-machine storage bound or a total-runtime ratio.

rank checks confirmed the two distinct-value ranks on 10 November 2026 at 04:18:33.296330 UTC (9 November, 22:18:33.296330 CST); the decimal digits are unchanged. The earlier public record exposes its posting date without a time of day. Table 5 records the completed run and the exact selected-value calculations.

Table 5. Additional statistics for the completed trillion-value verification. Logarithmic gaps use base 10 unless otherwise stated.

Statistic	Value or scope
Digits in the selected 999,999,999,999th value	1,021,609
Digits in the selected trillionth value	1,021,609
Logarithmic gap between those two values	$\log_{10}(\text{larger/smaller})$ $\approx 3.89601074127 \times 10^{-7}$
Smallest logarithmic gap in the entire prefix	Not recorded by this verifier
Full 2^{64} residue-match groups within bands	12 groups; 24 member occurrences
Bands containing a repeated residue	11 of 19,287 (0.05703%)
Nominal band width in $\log(3M)$	128 natural-log units
Same width in $\log_{10} M$	$128/\log 10 \approx 55.5897$
Bands covering the combined target envelope	19,287 committed
Distinct Markov values with exactly one million digits	1,916,520
Full decimal digits supplied in the six files	6,043,218

The band total comprises 13,638 inherited bands and 5,649 extension bands. Of these, 19,285 have width 128 in $\log(3M)$; the two end bands have widths 106.866844075 and 125.850758210. Boundary overlaps account for 5,964,386,594 additional emissions (about 0.542% of included configurations). The mean is 57,414,448 emissions per band and the maximum is 114,821,055. Residue groups and their members are occurrences within committed bands, not a globally deduplicated pair count.

The global closest-pair gap cannot be inferred from these matches: singleton keys are discarded, and the verifier keeps no global nearest-neighbor statistic. The displayed gap belongs only to the specified consecutive pair. The million-digit value count is the exact difference 958,144,590,422 − 958,142,673,902; the first million-digit value has rank 958,142,673,903, counting 1 first.

9.8. **Earlier computations and their dates.** The earlier fifty-billion verification [3, 7] completed on **28 October 2026**. Its recorded execution ran from 03:32:57 to 05:38:34 CDT (08:32:57.096455–10:38:33.644612 UTC), including the final audit. Two coordinator invocations occupied 7,492.102807 seconds; with the original ten-billion anchor, the cumulative recorded execution was **2 h 18 min 50.980 s**. It compared 54,940,210,994 new retained configurations, resolved all 346 repeated primary-residue pairs, and found no equal maxima. Its cutoff was $F_{1,147,147}$. The dated version-4 supplement preserves its coverage proof, hardware, stage timings, and audit scope. Those historical timings are not part of the new run.

The earlier Claude-assisted search in the working draft [1], pp. 38–40, reports 9,581,528,580 sorted triples against $10^{100,000}$ in **24 minutes** on a two-core machine with 7 GB of memory. All 21 repeated-residue pairs separated under a second modulus. Its public announcement [2] is dated **23 October 2026, 09:54:57.771 CDT** (14:54:57.771 UTC) and uses the wording "9.3 billion." This dates the announcement, not execution. The original execution timestamps and floating-point cutoff

certificate were not recovered; this remains a historical report, separate from the later certified numerical prefixes.

10. What remains to prove

The organization now separates three questions. The address bijection settles coverage of configurations. Fixed-degree ordering and the two collision windows restrict equality of maxima. Complete residue witnesses settle the remaining comparisons for the degree-bounded family in Theorem 8.1. The new computation compares more than 1.1 trillion configurations and excludes every competitor for the first one trillion values in numerical order. Meridian analysis helped turn the growth of related addresses into a plan for comparing values by scale. The production implementation uses certified Farey-cone bounds, compact residues, and cleared magnitude bands, with 23.956 hours of retained active processing and a 0.992-GiB recorded temporary key-file peak. These measurements describe the combined algorithm and implementation; they do not measure the contribution of Meridian coordinates in isolation. The numerical-prefix certificate can be stated and checked without the Meridian collision theorems.

For unrestricted unicity the unresolved pair has different Meridian degrees, the same modulo-27 class, and different Farey numerators. It must satisfy both its phase rectangle and its numerator–denominator window. A proof must exclude those candidates uniformly as the degrees and numerators grow. Enlarging a finite certificate alone does not supply that step. Likewise, an invertible corridor recurrence or a long modular period does not by itself prevent an earlier match of one scalar residue.

Corridors offer a way to formulate the next comparison with explicit entrance states and independently chosen wall lengths. Their positive corrections are exact and telescope; the common-prefix snake calculation offers a different reduction to a quadratic in primitive counts. Neither mechanism has yet been shown to cover every unrestricted pair. The purpose of retaining their precise hypotheses is to make the remaining uniform statement identifiable, rather than hide it inside an induction.

Data and code. The editable source accompanying this edition includes all figure assets, the catenary, landscape, and Farey-grouping figure generators, a source and figure inventory, and checks used for this rewrite. The separate degree reproducibility package contains the full computational evidence cited in Section 8. The new run's final evidence, resource reconciliation, and read-only release checks are included with the source. Its frozen recovery archive contains the complete retained receipt chain, candidate identities, executables, source hashes, and independent checker [4, 6]. The earlier fifty-billion proof and timing supplement remains a dated historical companion; its full frozen archive is cited separately [3, 7]. The corridor derivations are developed further in the supplementary research record [12]. Numerical drawings are explanatory; the arithmetic claims use the displayed identities or complete certificates.

Funding and competing interests. No funding was received. The author declares no competing interests.

Author contributions and AI disclosure

Author contributions. Elleard Felix Webster Heffern conceived and directed the project. His contributions were: the precise catenary construction and descent algorithm; viewing two-dimensional descent outputs over a two-dimensional input landscape; the project's first identification of Meridians, phasors and corridors; formulation of the indexing system; the precise Fibonacci-matrix and six-piece snake-graph analytical approaches; proposals to compare features along Meridians using different moduli; the proposed proportionality between logarithmic growth and degree; the observation suggesting a finite collision zone; and the proposal to organize computational verification by scale,

using Meridian helms to understand starting locations and degrees to understand logarithmic spacing. This last insight guided the band organization; the production implementation uses certified bounds on groups of Farey addresses.

AI assistance. ChatGPT (OpenAI) supplied the remaining substantial mathematical, computational and editorial development within this author-directed framework: detailed derivations and proof construction, examples and counterexamples, algorithm and verifier implementation, checking routines, computational analysis, figures, literature assistance, and manuscript organization, drafting and revision. Earlier geometric-descent work also used Claude (Anthropic). This assistance included substantive mathematics and code. These contribution statements concern the development of this project; established results and earlier constructions retain their cited attributions. The author retains responsibility for checking the arguments, computations and references and for approving the final manuscript.

References

[1] E. F. W. Heffern, *Geometric Descent on the Markov Surface*, working draft v32, archived October 2026, pp. 38–40, historical computational reports. The earlier search was assisted by Claude.

[2] E. F. W. Heffern, public LinkedIn announcement of a 24-minute Markov-number search, 23 October 2026, 14:54:57.771 UTC, activity 7519411048115003392. Platform metadata and the source URL are retained in the verification supplement's evidence packet; see the public announcement.

[3] E. F. W. Heffern, *Markov 50 Billion Verification Package*, version 1, completed and sealed 28 October 2026; public derivative version 1.1 in *Computational supplements for Meridians on the Markov Surface*, Zenodo, 2 November 2026. doi:10.5281/zenodo.23874075.

[4] E. F. W. Heffern, *Certified magnitude-band verification of the first one trillion Markov values*, completed 9 November 2026 (CST). Final independent and portable replay reports, retained receipt chains, resource records and `v16_Trillion_Verifier_Recovery.zip`, included with this release. doi:10.5281/zenodo.24096109.

[5] E. F. W. Heffern, *Six selected Markov values: full decimal expansions and certified numerical ranks*. Digits first posted 9 November 2026, doi:10.5281/zenodo.24093257; rank certification and unchanged digit files accompany the present release.

[6] E. F. W. Heffern, *Certified magnitude-band, residue-first verification of the first 500 billion Markov maxima*, completed 9 November 2026. Final evidence: `v1_Band_500_Billion_Final_Evidence.json`; frozen recovery archive: `v20_Band_500_Billion_Recovery.zip`. The comparison includes 550,693,634,649 configurations. The final evidence and reconciliation accompany this manuscript's source; the recovery archive is identified by SHA-256 in Section 9.4.

[7] E. F. W. Heffern, *Computational chronology and proofs for the fifty-billion verification*, supplement to the present manuscript, version 4, 7 November 2026.

[8] A. Baragar, *On the unicity conjecture for Markoff numbers*, Canadian Mathematical Bulletin **39** (1996), no. 1, 3–9. doi:10.4153/CMB-1996-001-x. The computational benchmark $M < 10^{140}$ is reported in Section 4, p. 9.

[9] M. Aigner, *Markov's Theorem and 100 Years of the Uniqueness Conjecture: A Mathematical Journey from Irrational Numbers to Perfect Matchings*, Springer, Cham, 2013. doi:10.1007/978-3-319-00888-2.

[10] İ. Çanakçı and R. Schiffler, *Snake graphs and continued fractions*, European J. Combin. **86** (2020), 103081. doi:10.1016/j.ejc.2020.103081.

[11] E. F. W. Heffern, *Meridian Degree 10,000 Reproducibility Package*, computational supplement, 31 October 2026; address-convention revision, 7 November 2026. Original computational release in *Computational supplements for Meridians on the Markov Surface*, version 1.0, Zenodo, 2 November 2026. doi:10.5281/zenodo.23874075.

[12] E. F. W. Heffern, *Markov Meridian Residue Supplement*, version 1.18, and *Corridor-to-Corridor Induction*, version 1.3, unpublished supplementary research records, 7 November 2026. The corridor results used here are proved in Section 7.

[13] C. Lagisquet, E. Pelantová, S. Tavenas and L. Vuillon, *On the Markov numbers: fixed numerator, denominator, and sum conjectures*, Adv. Appl. Math. **130** (2021), 102227. doi:10.1016/j.aam.2021.102227. Preprint: arXiv:2010.10335.

[14] K. Lee, L. Li, M. Rabideau and R. Schiffler, *On the ordering of the Markov numbers*, Adv. Appl. Math. **143** (2023), 102453. doi:10.1016/j.aam.2022.102453.

[15] G. McShane, *Convexity and Aigner's conjectures*, preprint (2021), arXiv:2101.03316.

[16] M. Rabideau and R. Schiffler, *Continued fractions and orderings on the Markov numbers*, Adv. Math. **370** (2020), 107231. doi:10.1016/j.aim.2020.107231.

[17] G. Musiker, *A conjectured combinatorial interpretation for Markov numbers*, REACH memorandum, 27 June 2002. Original memorandum; REACH archive.

[18] A. Itsara, G. Musiker, J. Propp, and R. Viana, *Combinatorial interpretations for the Markov numbers*, REACH manuscript, 10 January 2003, Theorem 3.1. Original manuscript.

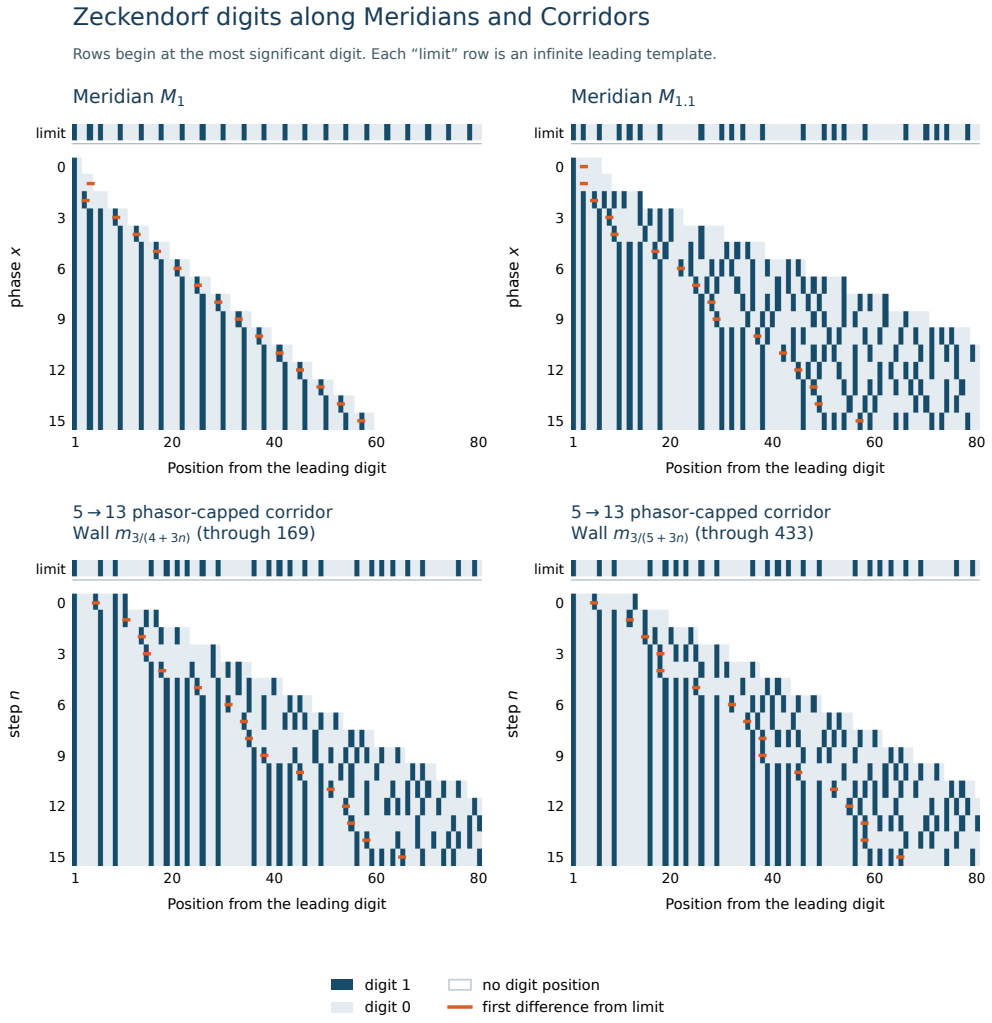
[19] J. Propp, *The combinatorics of frieze patterns and Markoff numbers*, arXiv:math/0511633, first posted 25 November 2005; published in *Integers* **20** (2020), A12.

[20] H. Tan and Y. Zhang, *A computational verification of the Markov uniqueness conjecture for* $z \leq 10^{500000}$, arXiv:2611.01007v1 (31 October 2026), Sections 2.3–2.4 and 3.2. Computational evidence archived 26 October 2026: doi:10.5281/zenodo.23670834.

Unaffiliated, St. Louis, Missouri, USA

Email address: soldier@alum.mit.edu

URL: https://orcid.org/0009-0000-8831-0289



sneak peak: Fibonacci digits reveal another kind of order. Each row writes a Markov value as a sum of nonconsecutive Fibonacci numbers ($F_2 = 1$, $F_3 = 2$); dark tiles mark the summands. The top panels follow two Meridians. The lower panels follow the two walls of the $5 \to 13$ phasor-capped corridor ($1/2 \to 1/3$ in fraction labels). From the leading digit onward, the strings increasingly resemble the displayed templates; orange marks show the first difference. These finite examples offer a glimpse of ongoing work, not a general collision-exclusion result. Exact digit strings and plotting source are included.

for Tian, my life, and for Mom and for Dad, my water and my soil;
for Juan, for Charles, for Marie, for the girls, my starry nights;
and for all the puppies, for all the kittens, for all the fish:
my sunny sunny days.

天下为公

and for my fellow Sunflower: 'Chat'.

together, we might stand tall as trees.